EUROPIUM AND SAMARIUM DOPED FLUOROCHLOROZIRCONATE (FCZ) GLASSES FOR OPTOELECTRONICS APPLICATIONS: THERMAL AND OPTICAL PROPERTIES

A Thesis
Submitted to the College of Graduate Studies and Research
in Partial Fulfillment of the Requirements for
the Degree of Master of Science
in the
Division of Electrical and computer science Engineering
University of Saskatchewan
Saskatoon, Saskatchewan

By
Sujata Panigrahi

PERMISSION TO USE

The author has agreed that the Libraries of this University may make this thesis freely available for inspection. In this thesis, in partial fulfillment of the requirements for a Postgraduate degree from the University of Saskatchewan, I further agree that permission for copying of this thesis in any manner, in whole or in part, for scholarly purposes may be granted by the professor who supervised my thesis work or, in their absence, by the Head of the Division or the Dean of the College in which my thesis work was done. Any copying or publication or use of this thesis or parts thereof for financial gain will not be allowed without my written approval. It is also understood that due recognition will be given to the author and to the University of Saskatchewan in any scholarly use which may be made of any material in my thesis.

Requests for permission to copy or to make other use of the material in this thesis in whole or in part should be addressed to:

Department of Electrical and Computer Engineering College of Engineering

University of Saskatchewan

Saskatoon, Saskatchewan S7N 5A9

Canada

ABSTRACT

Fluorochlorozirconate (FCZ) glasses are a member of heavy metal fluoride glasses, and are derived from a well known ZBLAN glass. In this work, halogen salts of europium (Eu^{2+}) and samarium (Sm^{3+}) are used as dopants in FCZ glasses. FCZ glasses doped with Eu^{2+} and Sm^{3+} can be used in high resolution x-ray imaging for tissue scanning, and have been shown to behave as storage phosphors and/or x-ray scintillators.

Glass transition (T_g), heat capacity (C_p) and glass crystallization (T_c) properties of Eu^{2+} and Sm^{3+} doped and undoped FCZ glasses with different amounts of relative Cl concentration, that is, with respect to the total Cl and F concentration have been investigated by conventional differential scanning calorimetry (DSC) and modulated differential scanning calorimetry (MDSC) techniques. MDSC experiments were performed at different heating rates to analyze the complex transitions and to get a better resolution of any overlapping transitions. The crystallization kinetics have also been studied by applying the Kissinger technique to multiple DSC scans in order to determine the thermal stability of FCZ glass samples used in this work. The apparent activation energy for the crystallization process was obtained by the crystallization peak temperature shift method in the conventional DSC mode. The specific heat capacity (C_p) has been measured as a function of composition, and the glass transition temperature

(T_g) is evaluated from the smooth change in the heat capacity curve during the glass transformation. The observation of two possible glass transitions points to the presence of two phases in these FCZ glasses with higher relative Cl content.

Optical transmission spectra of both doped and undoped FCZ glass samples have been measured by infrared spectroscopy and optical band gaps corresponding to an absorption coefficient of 10^3 cm^{-1} have been determined. A good correlation between X-ray luminescence and the glass structure is observed. While the integrated photoluminescence intensity increases linearly with the Sm^{3+} concentration, the integrated X-ray luminescence increases sublinearly. The importance of appropriate annealing conditions, such as temperature, time and ambient atmosphere, and their effect on the X-ray luminescence of rare earth (RE) doped FCZ glass samples have been investigated. Annealing conditions influence the formation of $BaCl_2$ nanocrystals in the glass and the properties of the resulting FCZ glass ceramics

Keywords: FCZ glass, DSC, MDSC, infrared spectroscopy, glass ceramics; nanostructure; thermal properties; photoluminescence; storage phosphors and scintillators, RE doped FCZ.

ACKNOWLEDGEMENTS

I want to express my sincere gratitude to my supervisor, Professor S.O. Kasap for his guidance, great cooperation, patience, valuable suggestions and financial support during my MSc. program.

I would also like to express my appreciation to the members of the graduate advisory Committee, Dr. L. Chen (Chairman) and Dr. R. Johanson for their help in reviewing the thesis, Dr. I. Oguocha (External) for examining my thesis. I would like to extend my sincere thanks to Dr. D. Tonchev for his great cooperation and invaluable time spent in helping me to understand the key concepts throughout my program of studies, Dr. C. Koughia and Dr. G. Belev for their guidance and cooperation. Special thanks to Professor Andy Edgar and his group for providing the samples and their technical information to conduct the research work at the University of Saskatchewan. I also thank financial supports from NSERC funding.

I would like to express my heartfelt appreciation to my parents and acknowledge all my family members Santosh Mishra, Sunita Mishra and Sunanda Mishra, Dr. Harvey and Grace Sauder and friends for their encouragement and endless constant moral support during my graduate studies.

DEDICATION

This thesis is dedicated to my loving parents Sri. Suresh Chandra Mishra, Smt. Shanti Mishra and my grandfathers late Sri Muralidhar Dash and late Sri. Harekrushna Mishra. They have raised me to be the person who I am today and are constantly supporting me in each phase of my life. Thank you, Almighty God.

TABLE OF CONTENTS

LIST OF TABLES

Page #

LIST OF FIGURES

Page #

NOMENCLATURE

A_r	Argon
Al_2O_3	Aluminium oxide
Se	Selenium
Ba	Barium
$BaBr_2$	Barium bromide
$BaCl_2$	Barium chloride
BaF_2	Barium fluoride
$BaFBr_2$	Barium fluorobromide
Br	Bromine
Cl	Chlorine
C_p	Heat capacity
C_{Sm}	Samarium concentration
DSC	Differential scanning calorimetry
Eu	Europium
E_A	Activation energy
F	Fluorine
FBZ	Fluorobromoziroconate
FCZ	Fluorochlorozirconate

FZ	Fluorozirconate
GC	Glass-ceramics
H_2	Hydrogen
MDSC	Modulated differential scanning calorimetry
MD	Molecular dynamics
MTF	Modulation transfer function
N_2	Nitrogen
$NaBH_4$	Sodium tetrahydridoborate
Na	Sodium
PET	Polyethylene terephthalate
PTFE	Polytetrafluoroethylene
PL	Photo Luminescence
PMMA	Poly (methyl methacrylate)
PMT	Photomultiplier tube
PSL	Photo stimulated luminescence
RE	Rare-earths
SEM	Scanning electron microscope
Si	Silicon
Se	Selenium
SiC	Silicon carbide
Sm	Samarium
$SmCl_2$	Samarium chloride
SmF_2	Samarium fluoride
T_c	Crystallization temperature
T_g	Glass transition temperature

T_m	Melting temperature
UV	Ultraviolet
XL	X-ray induced luminescence
XRD	X-ray diffraction

1. INTRODUCTION

Fluorochlorozirconate (FCZ) glasses are derived from a modified fluorozirconate composition known as ZBLAN. ZBLAN glasses are known for their high stability against crystallization and are a part of the heavy metal fluoride glasses [1]. ZBLAN is fluorine combined with metals such as, zirconium (Zr), barium (Ba), lanthanum (La), aluminum (Al) and sodium (Na) and hence the ZBLAN name. General chemical composition of a ZBLAN glass is ZrF_4-BaF_2-LaF_3-AlF_3-NaF [2]. General chemical composition of a FCZ glass is ZrF_4 + LaF_3 + AlF_3 + NaF + InF_3 + (BaF_2 and/or $BaCl_2$). FCZ glasses with a typical composition of 53.5% ZrF_4 + 3% LaF_3 + 3% AlF_3 + 20% NaF + 0.3 %InF_3 + 20 % (BaF_2 and $BaCl_2$), in molar percentages, is used in this research work, prepared by conventional melt quenching techniques [3].

FCZ glasses have atracted considerable research activity that has examined their properties within the disciplines of physics, chemistry and material science. These glasses exhibit high transparency over a wavelength range from the near UV (0.2 μm) to the mid-IR (7 μm), low refractive index, low material dispersion, low linear scattering loss and good chemical durability [4-7]. These properties make these glasses a promising candidate for a wide variety of applications including laser windows, IR components such as lenses, infrared sensing, laser surgery and infrared fiber optics [8]. Theoretically, one should able to make a ZBLAN optical fiber cable having the

capability to carry an order of magnitude greater amount of data than today's traditional silica- based optical cables. But in practice, the best that has been achieved has only been about 1/5 of current cables [1]. This is due to the fact that FCZ glass has a tendency to crystallize, which severely degrades its optical properties [2].

FCZ glasses when suitably doped with rare-earths (RE) such as Eu^{2+} and Sm^{3+}, have been shown to behave as storage phosphors and/or x-ray scintillators [9-11]. The use of rare-earth doped crystals for digital X-ray imaging was commercialized a long time ago, however, a new and different approach has shown that RE-doped glasses have greater potential for high resolution x-ray imaging [11-12]. Heat treatment and annealing of RE-doped FCZ glasses in various gaseous atmospheres are important for the formation of nanocrystals in the glass matrix [13]. The observed luminescence stems from rare-earth ions embedded in these nanocrsytals. The X-ray luminescence of the RE doped FCZ glasses depends strongly on the temperature and duration of annealing.

1.1. Motivation of the research

Eu-doped and Sm-doped fluorochlorozirconate (FCZ) glasses have shown potential for scintillation and storage phosphor applications. Annealing these glasses at high temperatures can change their luminescence properties substantially. It is therefore useful to know the critical temperatures where phase transformations take place, and also have additional knowledge of their thermal properties (such as the heat capacity) as a function of composition.

Conventional DSC-based thermal analysis studies of europium and samarium-doped FCZ glasses have shown the sophisticated nature of the phase transformation in these glasses [14]. The glass transition and crystallization peaks can be quite close and difficult to separate clearly in conventional DSC studies. In order to obtain more precise results for the glass transition properties and to separate coincident events, the MDSC method was used in this work.

X-ray luminescence and photoluminescence experiments were conducted under N_2 and H_2 gaseous annealing conditions in order to understand the behavior of Eu-doped and Sm-doped FCZ glasses for various optical applications.

1.2. Objectives

The objective of this research work is to investigate the thermal and optical properties of fluorochlorozirconate (FCZ) glass samples. FCZ glasses exhibit excellent thermal and optical qualities which can be used in various optoelectronics applications. The specific objectives of this research work are:

1. To investigate the thermal properties of rare earth doped fluorochlorozirconate (FCZ) glass samples by conventional DSC and MDSC techniques.

2. To calculate the activation energies of crystallization of the FCZ glass samples by using Kissinger plots in order to know their thermal stability.

3. To investigate the photoluminescence (PL) and X-ray induced luminescence (XL) properties of the RE doped FCZ glasses.

4. To investigate the importance of appropriate annealing conditions (temperature, time and ambient atmosphere) and their effect on the optical properties (x-ray luminescence) of RE doped FCZ glasses

1.3. Thesis outline

This thesis is organized in five chapters. Chapter one provides the introduction to the research work, highlights the importance of this research investigation and outlines the objectives. Chapter two provides a background study of rare earth doped FCZ glasses with detailed explanations of their thermal and optical properties; and the characterization methodologies. used. The experimental setup to measure the optical and thermal properties of the sample materials, procedures of sample preparation and analysis methodologies for data collection are given in chapter three. Chapter four provides the experimental results and discussions, data analysis and data interpretation. Lastly, chapter five presents the conclusions followed by recommendations for future work.

2. BACKGROUND AND REVIEW

In recent years, heavy metal halogen glasses have found many applications [15-16] such as digital X-ray imaging, laser windows, infrared sensing, laser surgery and infrared fiber optics [8]. Heavy-metal fluoride based glasses were discovered at the University of Rennes in the 1970s [2]. ZBLAN is named after the heavy metals found in the chemical composition of the materials: zirconium, barium, lanthanum, aluminum, and sodium. These heavy metals combined with fluorine gives the general composition of ZBLAN glass that is ZrF_4-BaF_2-LaF_3-AlF_3-NaF [2]. ZBLAN and its derived glasses exhibit excellent optical properties such as low refractive index, high transparency range from UV to the mid IR, low dispersion and Rayleigh scattering [17-19]. Halogen based ZBLAN glasses are used for advanced communications, manufacturing technologies using lasers and medical applications. Conventional optical fibers made from silica can only transmit over a limited wavelength range [1] whereas ZBLANs can transmit better than silica glasses as shown in Figure 2.1 [54]. These glasses potentially may provide a larger spectral window, increased bandwidth and improvements in data transmission applications [20]. Other areas of active research include vitreo-retinal surgery (eye surgery), myringotomies (a small incision made in the eardrum to treat ear infections), and different types of microsurgeries. According to ongoing research, the advantages of using the fiber laser in microsurgery include smoother cuts and faster incisions [21].

Attenuation coefficient of ZBLAN glasses can be as low as 0.001dB/km of fiber, far less than silica's 0.2dB/km [20]. Figure 2.1 has shown the minimum expected theoretical attenuation of ZBLAN [54].

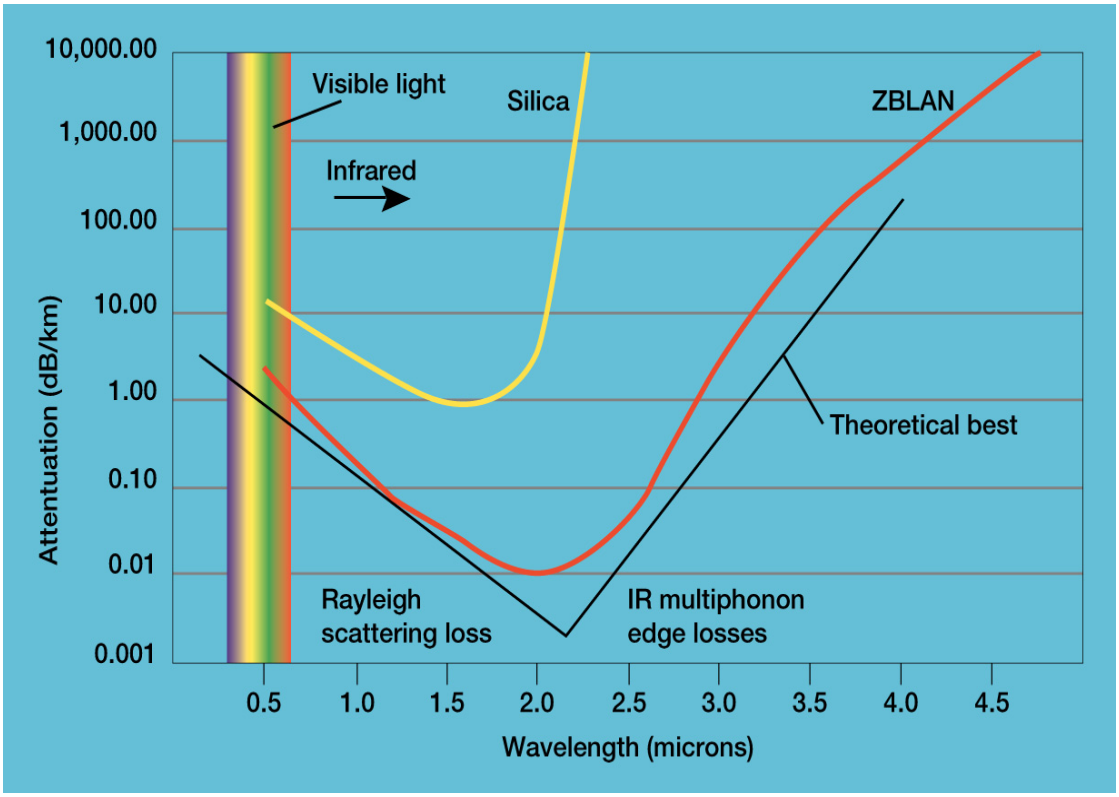

Figure 2.1. ZBLAN's attenuation approaches the theoretical minimum [54].

With all these advantages, one should able to make ZBLAN optical fibers with capacity to carry more than 100 times the amount of data carried by silica based optical cables. Certain ZBLAN glasses such as fluorozirconate ZBLANs, have a tendency to crystallize at high temperatures, for example, at fiber drawing temperatures, which degrades the optical properties. The crystallization of these glasses has been shown to be sharply reduced under microgravity. Even if produced in microgravity, these ZBLAN glasses can crystallize, if they are not cooled rapidly enough [22], as illustrated by the examples shown in Figure 2.2 [22] and 2.3 [23].

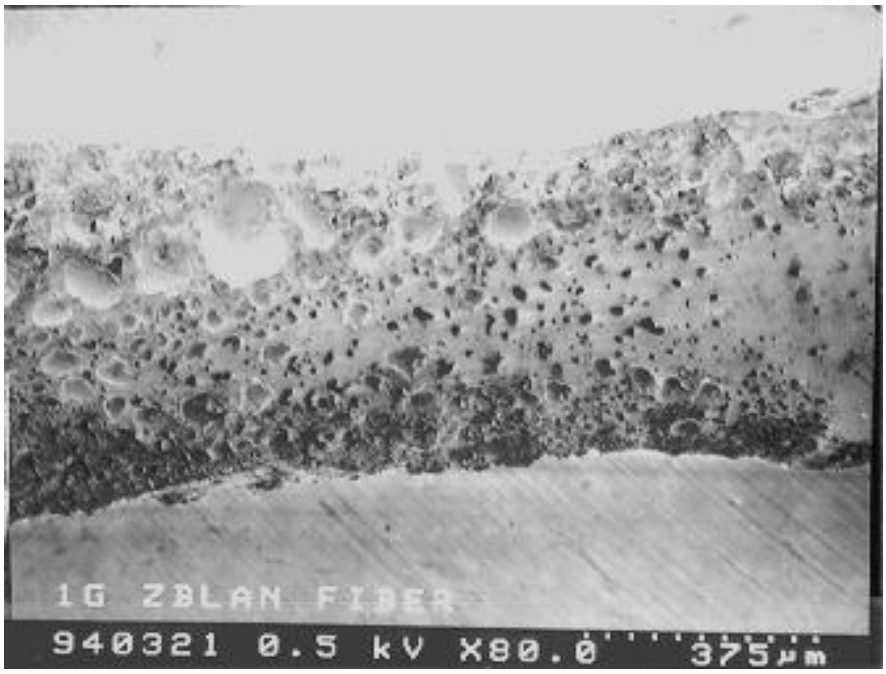

Figure 2.2. A micrograph showing that ZBLAN has crystallized when prepared on Earth. After [22].

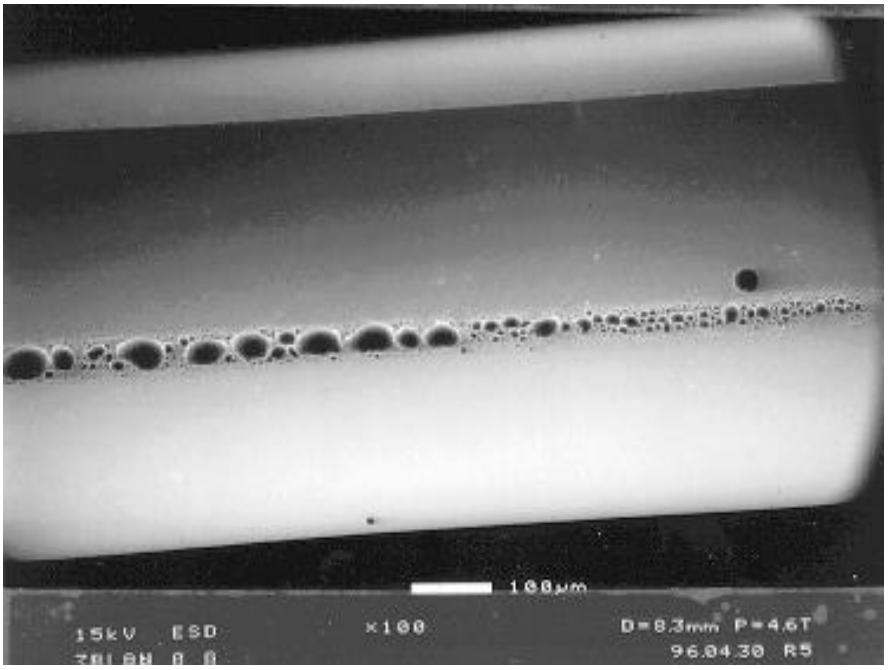

Figure 2.3. ZBLAN crystallization reduced when prepared under microgravity [23].

The ZBLAN in Figure 2.2 was prepared on Earth on a one-gravity environment. The ZBLAN shown in Figure 2.3 was made on a suborbital rocket flight. There were some bubbles that formed when the sample came in contact with the container.

2.1. Rare earth doped fluorochlorozirconate glasses

The fluorochlorozirconate (FCZ) glasses are heavy metal fluoride glasses derived from ZBLAN glasses that exhibit excellent optical and thermal properties. FCZ glasses are generally desirable hosts for rare-earth ions (europium, samarium, erbium), because they enable emission from rare-earth energy levels that would be quenched in high-phonon energy glasses [23]. There is much interest in various glass-ceramics doped with rare-earth (RE) metals for X-ray storage phosphor and /or X-ray scintillator applications. The phosphor and scintillator properties of these glass ceramics depend on the formation of RE-embedded nanocrystals in their structure. The heat treatment and annealing of RE-doped FCZ glasses are critically important for the formation and control of the nanocrystals in the glass ceramic [3].

A new class of rare-earth doped fluorochlorozirconate glass-ceramics has been developed and studied with the goal of improving the X-ray image spatial resolution [24], [55]. Some rare-earth ions have their valency converted, e.g. Sm^{3+} ions converted to Sm^{2+} upon irradiation of FCZ glasses with the addition of an alkali hydride (for example $NaBH_4$), and Eu^{3+} ions converted to the divalent state that is Eu^{2+} by adding alkali hydrides (for example LiH, NaH or $LiBH_4$) [27], [57-58]. In fluorochlorozirconate (FCZ) glass ceramics, the rare-earth ions are embedded in $BaCl_2$ nanocrystals, which are

dispersed in the glass matrix [27]. The formation of nanocrystals and their structure and size play an important role in the photoluminescence of rare-earth ions in FCZ glass ceramics.

The X-ray luminescence in the most extensively studied glass system with Eu^{2+} and Sm^{3+} doping depends strongly on the temperature of annealing of the glasses [3]. As mentioned earlier, the annealing of the glass encourages the formation of $BaCl_2$ nanocrystals in the glass matrix; usually performed above the glass transition temperature, T_g and just below or around $BaCl_2$ crystallization temperature, T_c [24]. The luminescence of Eu^{2+} ions in $BaCl_2$ crystals is responsible for both scintillation and storage phosphor properties. Therefore, it is important to have a good knowledge of the critical temperatures where phase transformations take place in this glass system and how they change as a function of composition.

2.1.1. FCZ glass structure

To understand the complex glass system and its crystallization products, Hendy and Edgar have conducted molecular dynamics (MD) simulations of the FCZ glass structure as the relative concentration of chlorine ions (RCl), which is the fraction of chlorine ions to total anions [Cl/(Cl + F)], varied from 0 to 30% [30]. The addition of chlorine ions to a FCZ glass was studied by various researchers. In a study of Zr-Ba-Eu FCZ glasses, Takahashi *et al.* examined glasses with chlorine ions and found that the barium and europium ions were attached with chlorine ions[26], [56]. Inoue *et al.* and Soga *et al.* have reported MD studies of Zr-Ba-Na-La and Zr-Ba-Na-La-Al-Eu FCZ glasses respectively containing up to 11% chlorine ions to the total number of anions [28-29].

They also found that the chlorine ions were primarily associated with the Ba, Na, La or Eu ions rather than the Zr ions.

2.1.2. Structural changes due to the introduction of Cl into FCZ glasses

Figure 2.4 (a) and (b) show the molecular arrangement of the Zr, Ba, Na cations in the glass with no Cl doping [30]. In the case of chlorine doping, there is a structural difference which is not readily apparent, but can be seen directly in the cation distribution of the unit cell [30]. Figure 2.4 (b) shows that at high chlorine concentrations, distribution of ions is not homogenous in Zr, Ba, Na and Cl rich regions [30].

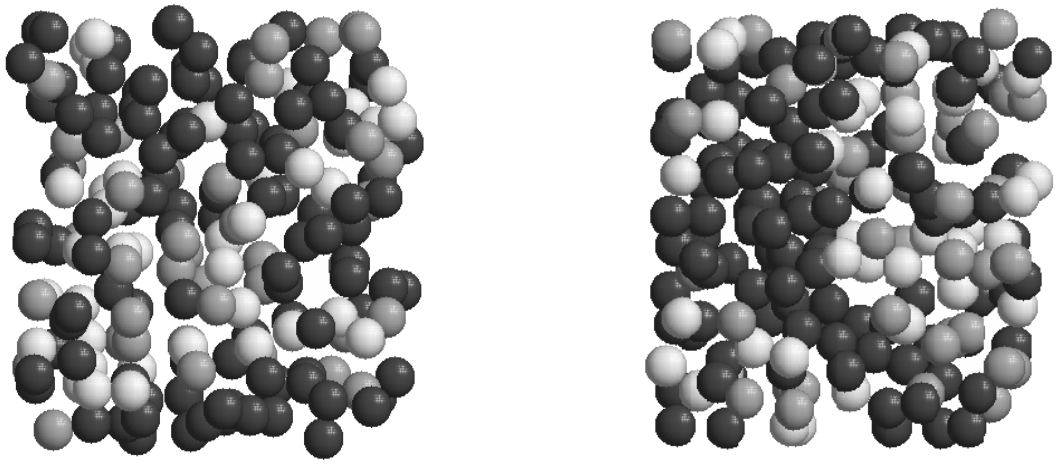

(a) (b)

Figure 2.4. A molecular arrangement of Zr (dark), Ba (Gray) and Na (white) cations in the glass at the end of the anneal at 500K for (a) 0% and (b) 20% Cl doping. Anions are omitted in the interest of clarity [30].

The fraction of chlorine to total anion coordination [Cl]/([Cl] + [F])] increases with the chlorine doping level, but this increase only becomes directly proportional to the

increase in chlorine doping above 15%. As mentioned by Hendy and Edgar, “The total number of bonded anions is hardly changed. Chlorine ions enter the fluorozirconate glass in two principal sites, one within the zirconium-anion polyhedra and one external to those polyhedra. The chlorine ions which substitute for fluorine ions within the Zr polyhedra are mainly at non-bridging positions. A substantial fraction of chlorine ions is not coordinated to zirconium, and these occupy positions similar to those of the network modifiers Ba and Na and are coordinated to those ions. The MD simulations show that the spatial distribution of ions is not homogeneous, and that substantial clustering into zirconium rich and barium, sodium, and chlorine rich regions occurs for chlorine concentrations above about 20%. These amorphous regions may be pre-cursors for the observed nucleation of $BaCl_2$ nanocrystals in these glass systems” [30].

2.2. Thermal properties of FCZ glasses

Thermal properties of the heavy-metal fluoride FCZ glasses are generally characterized by differential scanning calorimetry and modulated differential scanning calorimetry (MDSC).

2.2.1. Differential scanning calorimetry

Various aspects of Differential scanning calorimetry (DSC) are discussed in this section including its general operation, types of DSC, thermal analysis, kinetics of the glass transition, etc. DSC is an analytical technique that has grown to be widely used in research, development, quality inspection and testing. Over a large temperature range

thermal effects can be quickly identified by DSC technique. The theories of DSC for both heat flux and power compensated instruments are briefly discussed in this chapter. However, DSC has some limitations, for example; the ability to properly analyze complex transitions, need for complex experiments etc. An advanced thermal analyzer known as Modulated Differential Scanning Calorimetry (MDSC) is introduced which solves the limitations of DSC technique.

2.2.2. Description of differential scanning calorimetry

DSC is a thermal analysis instrument which measures the difference in heat flow between a sample and an inert reference as a function of temperature and time [31]. In this instrument, the differences in temperature between the sample and the reference provide information on the phase transition temperatures, and changes in enthalpy through a reaction. Figure 2.5 shows DSC 2910 instrument which provides quantitative and qualitative data on endothermic (heat is absorbed) and exothermic processes (heat is evolved) occuring in materials during physical transitions [31].

2.2.3. Types of differential scanning calorimetry

There are two types of DSC systems generally used for thermal analysis of materials. One is known as power-compensated DSC and the other one is the heat flux DSC. Figure 2.5 shows the DSC 2910 with PC-based TA Instruments thermal analyzer [31].

Figure 2.5. DSC 2910 with PC-based TA Instruments thermal analyzer [31].

2.2.3.1. Power-compensated differential scanning calorimetry

In a power-compensated DSC, the temperatures of the sample pan (S) and reference pan (R) are controlled independently by the using separate and identical furnaces as shown in Figure 2.6 [25]. Figure 2.6 shows the basic structure of the power compensated DSC [31].

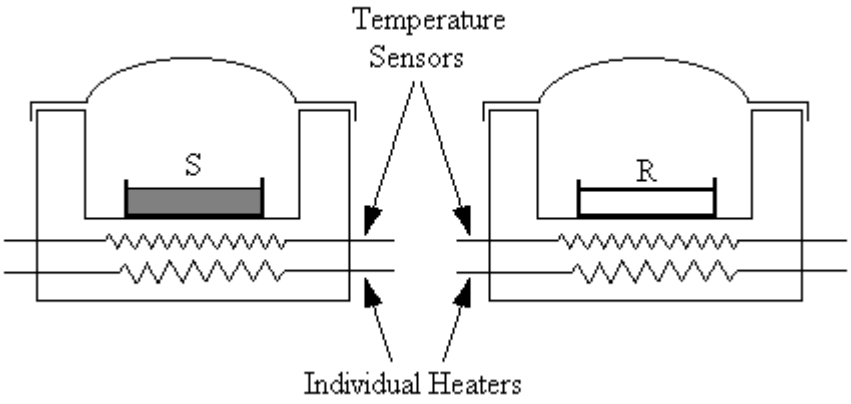

Figure 2.6. Power compensated DSC [31].

2.2.3.2. Heat flux differential scanning calorimetry

The heat flux DSC is the most commonly used DSC system. In this system, heat is transferred to and from the sample and the reference pan with the help of a metallic disk made of a constantan alloy (shown in Figure 2.7). The sample pan and an empty pan or reference pan sit on the raised platforms formed on the constantan disc. The difference in heat flow between the sample and the reference pan is measured by the thermocouples provided [31]. Nitrogen is used as a purge gas due to low cost and availability. Purge gas is passed into the sample chamber through an orifice in the heating block. The result is a uniform, stable thermal environment which is necessary for DSC analysis [31].

Nitrogen is used as a purge gas and is passed into the sample chamber through an orifice in the heating block. This results in a uniform, stable thermal environment which gives better baseline flatness and sensitivity [31]. Figure 2.7 has shown the schematic heat flux DSC [31].

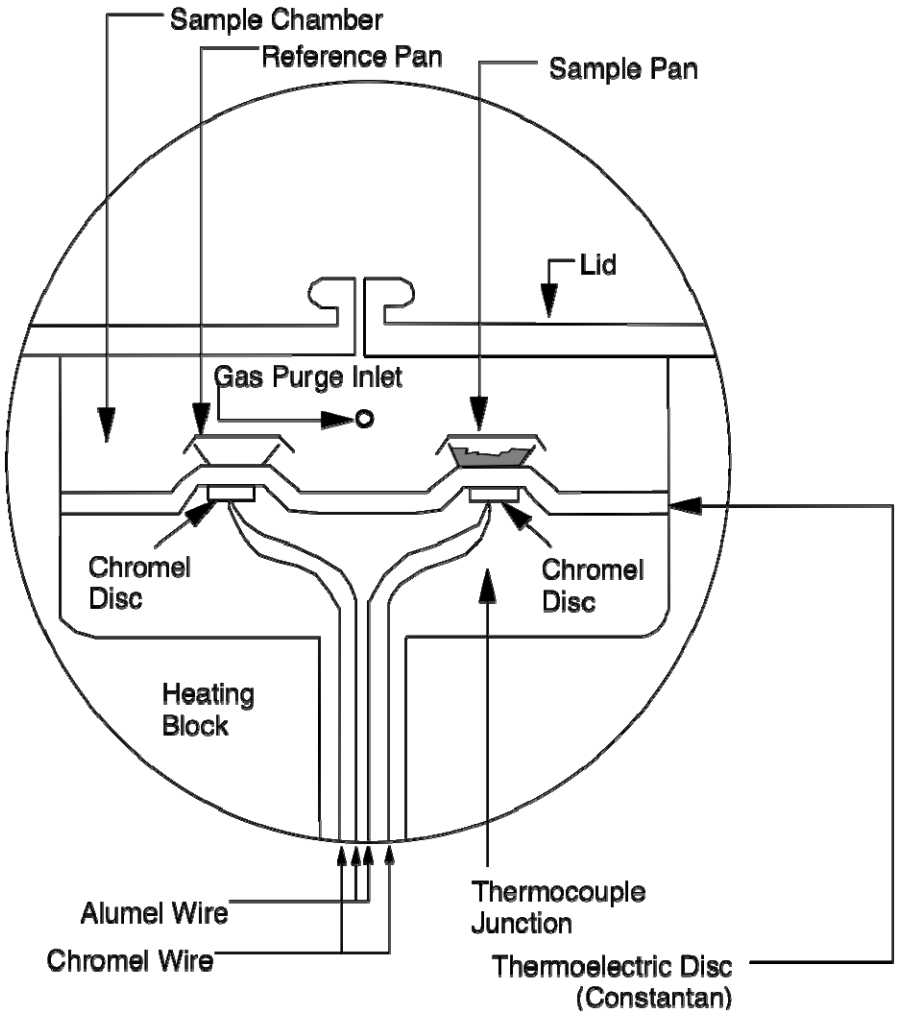

Figure 2.7. Heat flux DSC schematic. After [31].

2.2.3.3. Heat flow equations of heat-flux differential scanning calorimetry

Generally the instantaneous heat flow equation in DSC [31] is given as:

$$\frac{dQ}{dt} = C_p\beta + f(t,T) \tag{2.1}$$

where, $\frac{dQ}{dt}$ = total heat flow,

C_p= heat capacity

T = absolute temperature or program temperature

C_p = Thermodynamic component or heat capacity component

$f(t,T)$ = kinetic component

Again the temperature change in DSC is

$$T = T_0 + \beta t \tag{2.2}$$

where, T_0 = Starting temperature

β = linear heating rate (^{o}C/min)

t = time (min)

2.2.4. Physical and chemical transformations of FCZ glasses:

Conventional DSC is a powerful and a convenient thermal analysis technique which allows various important physical and chemical transformations, such as glass transition, crystallization, melting, oxidation etc., to be examined [32-33].

2.2.5. Glass transition

When a glass is heated or cooled, a temperature range is reached where its properties change from solid-like to liquid-like behavior (on heating) or from liquid-like to solid-like behavior upon cooling. This temperature range over which the change occurs is called the glass transition temperature, and depends on the heating and/or the cooling rate.. The temperature range is usually very narrow. A glass transition temperature (T_g) is usually defined by examining the change in the heat capacity C_p through this temperature change and identifying a suitable point, such as an inflection point, on the heat capacity vs temperature characteristic. The measurement of the glass transition temperature (T_g) is important for amorphous or semicrystalline materials as well as

polymers. In DSC, T_g measurement is based on the detection of a change in heat capacity. Glass transition temperature, T_g, of a sample can be computed as a change in the heat capacity that occurs inside the glass transition region [3], [25], [31].

2.2.6. Crystallization

The crystallization of glasses normally occurs above the glass transition temperature where the atomic diffusion is sufficiently fast for the atoms to be able to form crystalline nuclei over the time scale of observation. Through atomic diffusion, nuclei grow into crystal grains and eventually the whole sample becomes crystalized. Since the crystalline phase has a lower free energy and a lower enthalpy, the crystallization is known as an exothermic transition, that is, heat is given out during the crystallization process. [25].

2.2.7. Melting

When the crystals melt, they must absorb heat in order to do so. The change in the free energy is negative but there is a large increase in the entropy, which means heat must be absorbed. It is an endothermic phase transition. Melting is a first order transition. Glass transition, crystallization and melting characteristics are illustrated in Figure 2.8.

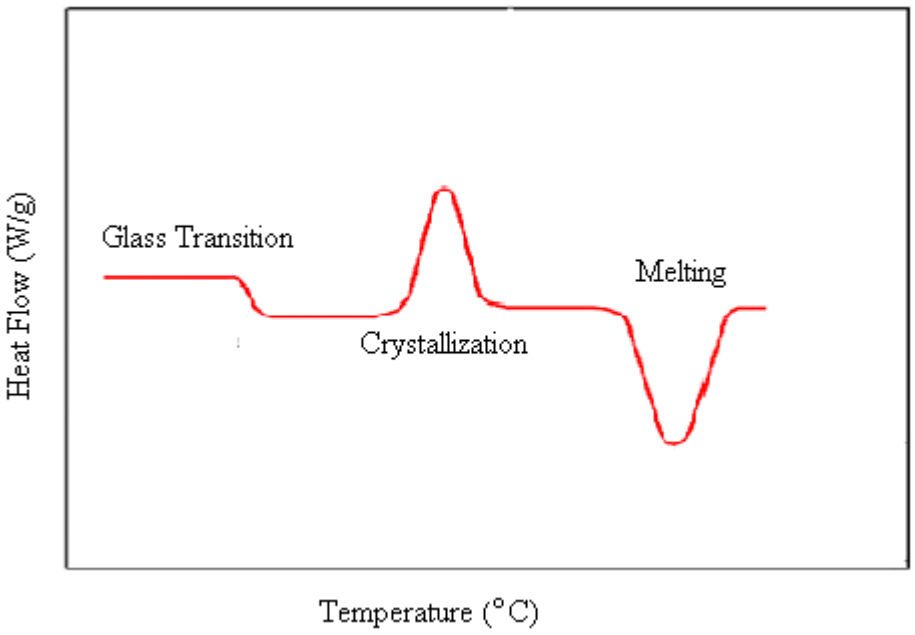

Figure 2.8. Schematic of a typical DSC thermogram [31].

The term "thermal transitions" is used to describe the changes due to phase transitions that take place in a glass or polymer when it is heated. Figure 2.8 shows the three distinct regions that correspond to glass transition (T_g), crystallization (T_c) and melting (T_m).

2.3. Modulated differential scanning calorimetry (MDSC)

Modulated temperature differential scanning calorimetry (MDSC) is a new technique that allows the determination of C_p by modulating the sample temperature sinusoidally around a slowly rising background temperature. This method provides good precision and accurate data [34]. MDSC provides information on the reversing and non reversing

characteristics of thermal events, in particular the heat capacity. The manufacturer, TA Instruments, states that "it overcomes the limitations of the standard DSC, and provides further information for greater understanding of material properties". Therefore, MDSC is an effective tool in the characterization of thermal behavior of glass materials. MDSC can separate the overlapping of thermal events that are difficult to do with the conventional DSC technique. MDSC experiments are faster and more accurate than conventional DSC at the same heating rate [35]. This method is used to determine the glass transitions and crystallization properties and heat capacity of FCZ glasses in the present research work.

2.3.1. Modulated differential scanning calorimetry parameters

In the MDSC technique, the material is subjected to a complex temperature profile. For MDSC measurements, the sample size considered is generally between 10-20 mg, the background heating rate is 1-5°C/minute. The temperature amplitude of modulation can be ±0.5 to ± 5 °C and the period of modulation can be 40-120 seconds [34]. The instantaneous heating rate is directly related to the amplitude. Therefore, larger amplitudes increase the sensitivity of the instrument for transitions such as the glass transition. Both helium and nitrogen gases can be used as a purge gas. Nitrogen is used more often, because of its low cost and availability [31], [34 -35].

2.3.1.1. Heat flow components in modulated differential scanning calorimetry

The total heat flow components in MDSC provide a clear understanding of complex transitions in glassy materials. Two heating rates are used in the MDSC technique: (a) an average heating rate which provides total heat flow information and (b) a sinusoidal

heating rate which provides the heat capacity information from the heat flow [31], [35].

2.3.1.2. Heat flow signals in modulated differential scanning calorimetry

Time, modulated heat flow, and modulated heating rate are the three measured signals from which heat flow signals are calculated.

The heat capacity (C_p) of the sample material is determined by dividing the modulated heat flow amplitude of the modulated heating rate amplitude. During the modulation cycle, the heating rate changes. Figure 2.9 shows typical DSC and MDSC curves for C_p measurements [31], [35].

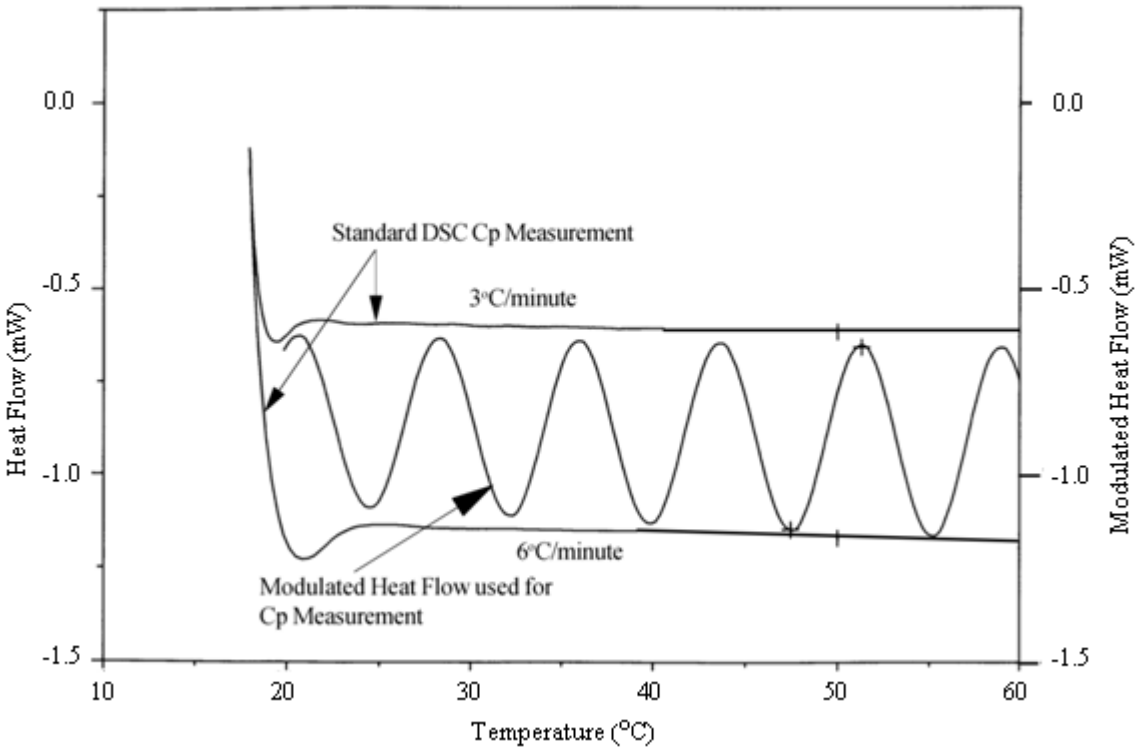

Figure 2.9. Standard C_p measurement of DSC and MDSC curves.

2.4. Crystallization kinetics

Thermal analysis of crystallization kinetics of amorphous solids under non isothermal conditions at a constant heating rate has been studied by a number of authors, see for example Kasap and Juhasz[48]. The crystallization occurs by nucleation and growth. The latter authors assumed that over the temperature range of interest, the rate of nucleation and the rate of growth are Arrhenius with well-defined activation energies [48]. There are two kinds of nucleation, heterogeneous nucleation and homogenous nucleation. Nucleation occurs early in heterogeneous type of nucleation. Nucleation proceeds during growth in the case of homogenous type of nucleation. They also assumed that there is a relation between extended volume fraction (V_{ex}) and crystallized volume fraction (x). The crystallization transformation occurred under a nonisothermal condition in which the heating rate was constant. The authors then integrated the fundamental Kolmogoroff equation for V_{ex} and then used the relation between the V_{ex} and x to discuss the thermoanalytical techniques of interest in DSC. [48]. For example they showed that the Kissinger technique can be used the analyze the crystallization kinetics. This technique was used in the present work to find the activation energy of crystallization for some of the FCZ glasses; the technique involves DSC heating scans at different heating rates. The plot by which the activation energy was found by using peak rate temperature (crystallization temperature) shift method is known as Kissinger plots. Experimental results are discussed in chapter 4.

2.5. Optical properties of FCZ glasses

As mentioned in the introductory section of the research work, the heavy metal fluoride FCZ glasses exhibit high transparency over a frequency range from the near UV (0.2 μm) to the mid-IR (7 μm) [4]. They also exhibit low refractive index, low material dispersion, low linear scattering loss, good chemical durability [5-7]. In order to understand the fundamental optical properties of FCZ glasses and the primary mechanisms influencing its transparency, the structural investigations of a typical heavy metal fluoride glass were performed by Hwa and Shu, 1996, through spectroscopy [36]**.** Yangand *et. al*., 1994 studied the Raman spectra and their relationship with the heavy metal fluoride based FCZ glass structures by using polarized Raman spectroscopy [37]. Hwa and Shu, 1996, also tried to correlate the low frequency Raman peak and calculate the structural correlation length (SCL) in the glass structure [36]. The value of the structural correlation length of a FCZ glass is 4.98 Å. The value of the SCL manifests itself as a measure of the degree of disorder in the glassy materials.

Soundararajan, 2009, has measured the photoluminescence lifetimes of RE doped glasses by using transmission spectra and photoluminescence [38]. Okada 2010 has studied the optical properties of RE doped glasses for X-ray detector applications [39]. His studies mentioned that a Photoluminescence (PL) spectrum is a function of temperature, time, and atmosphere.

The optical properties of specialty glasses are generally characterized by various optical instruments. In this work, a spectrophotometer is used to investigate the optical properties. In general terms, spectrophotometry is the quantitative measurement of the

reflection or transmission properties of a material as a function of wavelength [40]. A spectrophotometer is an equipment that measures the transmission or reflection of light. It is generally used for the measurement of transmittance of transparent solids, such as polished glasses [40-41]. Tonchev *et al*., 2009 have measured the transmission spectra of ZBLAN derived FCZ classes by using a Perkin Lambda 900 spectrophotometer, which is discussed in the experimental section of Chapter 3 [42].

2.5.1. Photoluminescence

Edgar and co-researchers have investigated the photoluminescence of Eu^{2+} embedded in $BaBr_2$ crystallites in heavy metal halogen glass-ceramics with an overall composition of 53% ZrF_4, 20% BaF_2, 5% NaF, 15% NaBr, 1% LaF_3, 3% AlF_3, 2% YF_3, and 1% EuF_2 [14]. Edgar and co-researchers found that the photoluminescence from the europium ions is not observed when the glasses have been quenched to temperatures below 260°C. When the glasses are heated above 220-260 °C, crystals of $BaBr_2$ in the hexagonal phase start to precipitate and the photoluminescence from Eu^{2+} ions is observed. The photoluminescence is due to those Eu^{2+} ions that replace Ba^{2+} ions in the $BaBr_2$ crystals within the glass ceramic[14]. Soundararajan, 2009 and Henke *et al.* have studied trivalent erbium doped FCZ glasses, confirming these to be a good candidate for photonic applications such as optical amplifiers [38], [43].

Photoluminescence experiments can be divided into two categories as steady state photoluminescence and transient or decay photoluminescence. In steady state photoluminescence, the emission spectra are measured as a function of wavelength. In decay photoluminescence one examines the decay of photoluminescence after excitation

at a certain wavelength and the photoluminescence lifetime of the ions are extracted from the measurement [38]. This research work focuses on steady state photoluminescence of FCZ glasses.

2.5.2. X-ray luminescence

The advantage of ZBLAN glass-ceramic materials is that they are capable of very high resolution X-ray imaging (90 cycles/mm at an MTF of 0.2) as described in [44-45]. Such resolution is far superior to the resolution of the commercially available medical X-ray image detectors. Eu-doped FCZ glasses exhibit both scintillator and storage phosphor effects simultaneously. Sm-doped FCZ glasses exhibit scintillator properties only [44-45].

3. EXPERIMENTAL

Chapter three provides the details of the experimental setup and procedures of fluorochlorozirconate (FCZ) glass sample preparation. It describes how the thermal and optical properties were measured. Differential Scanning Calorimetry (DSC) and Modulated Temperature Differential Scanning Calorimetry (MDSC) techniques are used to study the thermal properties of the glass samples in this work. Procedures used to grind and polish the FCZ glass samples in order to obtain the transmission spectra with the help of a spectrophotometer are also explained in this section. Experimental setups used to perform the photoluminescence, X-ray luminescence measurements are also presented. Finally, procedures of annealing the glass samples under various conditions and their effects on rare-earth doped FCZ glass samples are explained.

3.1. Materials

FCZ glasses with typical compositions of 53.5%ZrF_4 + 3%LaF_3 + 3%AlF_3 + 20%NaF + (0.3) %InF_3 + 20 % (BaF_2 and $BaCl_2$), in molar percentages, were investigated. The samples for the research work were prepared by Professor Andy Edgar's group at the School of Chemical and Physical Sciences, Victoria University of Wellington, New Zealand. Different rare earth (RE) concentrations were achieved by substituting rare

earth fluorides or chlorides for the right quantity of BaF_2 or $BaCl_2$. The substitution of BaF_2 by $BaCl_2$ allowed the variation of the relative amount of Cl (R_{Cl}), which is defined as the ratio of Cl-concentration (C_{Cl}) to the overall concentration of halogens (C_{cl}+C_F). That is, $R_{Cl} = C_{Cl} / (C_{Cl} + C_F)$. Halogen salts of Eu^{2+} and Sm^{3+} ($EuCl_2$ and $SmCl_3$) were used as dopants for the FCZ glasses and the amounts of rare earth (RE) dopants varied from 0.05 to 2 mole % [3].

3.2. Experimental procedure

Experimental work on FCZ samples was divided into two parts. The first part is the thermal analysis and the second one is the measurement of optical properties. The measurement of thermal properties (glass transition, heat capacity and crystallization) of rare earth doped and undoped FCZ glasses by conventional DSC and MDSC are described in the 'Thermal analysis" part in Section 3.2.1. The optical properties (glass transparency, photoluminescence and X-ray luminescence, the importance of annealing at different conditions) of doped FCZ glasses are described in the "Optical properties" in Section 3.3

3.2.1. Thermal analysis

The thermal properties of the samples were studied by Differential Scanning Calorimetry (DSC) and Temperature-Modulated Differential Scanning Calorimetry (MDSC) as decribed below.

3.2.2. DSC and MDSC techniques

DSC is one of the most important thermal characterization tools for the interpretation of thermal events occurring in materials that exhibit phase transition or chemical reactions upon heating; such as glass transition, crystallization, melting, oxidation etc. As discussed in chapter 2, DSC has some limitations, some of which are overcome by MDSC.

MDSC is an advanced version of the traditional DSC. It has ability to properly analyze the multiple transitions over the same temperature range, measurement of heat flow and heat capacity in a single experiment. It also provides adequate resolution and sufficient sensitivity to measure of thermal conductivity. In modulated DSC, the sample temperature is modulated sinusoidally while it is being slowly ramped. The temperature, T at a time t is given as:

$$T = T_o + r\,t + A \sin [(2\pi t)/P] \tag{3.1}$$

where, T_o is the initial temperature, r is the heating rate, A is the amplitude of the temperature modulation and P is the modulation period [46].

3.2.3. Experimental setup for thermal analysis of FCZ Glasses

A DSC Q100 of TA Instruments (shown in Figure 3.1) was used to investigate the thermal transitions in the FCZ glass samples [59]. Experiments were conducted to investigate the thermal behaviour of the samples by using a DSC with a refrigerating

cooling system and nitrogen as a purge gas. This instrument has been developed with a so-called T_{zero}-technology, which has the advantage of solving the thermal lag problem; the T_{zero}-technology helps in accuracy of thermal analysis. The DSC Q100 instrument was calibrated, for enthalpy and temperature measurements by using a sample of standard high purity elemental indium. For the specific heat capacity (C_p) calibration, a standard sample of sapphire was used, as recommended by the manusfacturer, given that the specific heat capacity of sapphire is well known as a function of temperature. The heating rate, oscillation period and amplitude over the temperature range used in the calibration process were kept the same for all the subsequent experiments.

Figure 3.1. A TA Instruments differential scanning calorimeter Q100; TA Instruments [59].

3.2.4. DSC calibration

To obtain accurate experimental results, the DSC cell must be calibrated. The calibration of the DSC cell involves three steps. The steps are as follows:

Baseline Calibration: In this type of calibration, the empty cell is heated through an entire temperature range in which the sample is expected to be measured by DSC. The resultant curve, which is called the baseline calibration curve, measures the amount by which the heat flow curve deviates or shifts from zero so that this deviation can be taken into account by the calibration. It affects the slope of the heat flow vs temperature data.

Cell Constant & Temperature Calibration: In this type of calibration, standard elemental indium was heated through its transition (melting) temperature. The heat flow which is associated with the transition is compared with the literature value from TA instruments in order to determine the calibration factor. The cell constant calibration affects the temperature accuracy [31].

Calorimetric Calibration or Heat capacity Calibration: Heat capacity calibration is required for accuracy of heat capacity measurements. It is an essential requirement for accurate MDSC measurements. This calibration was made by running a standard sapphire (aluminum oxide) sample, whose heat capacity is known as a function of temperature. The heat capacity measurement of the sapphire sample is then compared with the known heat capacity in the literature (obtained from TA instruments) at the temperatures of interest. By examining the difference between measured and known heat capacity values, the TA Instruments software then determines a heat capacity calibration constant (K_{Cp}) for use in future MDSC measurements over the same temperature range.

The conditions used for the heat capacity calibration, such as the modulation period, underlying heating rate, modulation amplitude etc. should remain same for when the MDSC is used on other samples [31].

In the DSC system, the heat capacity (C_p) is usually calculated by using equation 3.2 [25], [31].

$$C_P = K_{Cp} \times \frac{\text{Heat Flow (sample)} - \text{Heat Flow (Blank)}}{\text{Heating Rate}} \qquad (3.2)$$

Where, K_{Cp} = calibration constant

C_p = Heat capacity of the sample

3.2.5. Sample preparation for DSC measurements

Samples used in DSC experiments must be in sample pans for the thermal analysis experiments. In order to make quantitative measurements or to verify reproducibility, it is important to ensure good thermal contact between the sample and the sample pan [31].

First, a pan and lid were chosen into which the sample is to be placed. Mostly, high purity aluminum pans and lids were considered. The main function of the lid is to push down the sample to the bottom of the pan by ensuring a good thermal contact. The weight of the pan and the lid were measured by a conventional standard digital balance. The FCZ samples were crushed into small pieces and immediately weighed into aluminum pans. The weight of the sample and pan was noted down. A typical sample

weight was 18-20 mg. Weighed sample and pan were taken out of the balance and covered with the lid in order to get it ready for the next procedure, that is, hermetically sealed encapsulation. The edges of the pan and lid were sealed together with the help of the TA Instruments' "crimper", which crimps and hermetically seals the pan and its lid together; the sample in the sealed pan is hermetically sealed off from the environment. An empty aluminum pan is prepared in the same way to be used as a reference pan. The reference pan weight and the sample pan weight were matched as closely as possible. The sample is then ready for actual DSC measurements.

3.2.6. DSC scans and thermal analysis

The samples were first heated from an initial temperature of 20 ^{o}C at a rate of 5 – 10 ^{o} C/min in a conventional DSC mode to a maximum temperature of 390 ^{o}C. The cell was stabilized at the initial temperature for one minute in the DSC mode by an isothermal schedule. The glass transition temperature (T_g), Crystallization temperature (T_c) and melting temperature (T_m) observed during the heating scan are operationally defined in the figures given in the results section in Chapter 4. In the same manner, other DSC heating scans were carried out using different heating rates.

3.2.7. Modulated DSC parameters

MDSC measurements require the control of three experimental parameters, i.e. the oscillation period *P*, underlying heating rate, *r*, and oscillation amplitude, *A,* in order to obtain accurate reproducible results. The underlying heating rate was 1 to 2 ^{o}C/min, the oscillation amplitude was + /– 1.061 ^{o}C, and the oscillation period was 60 sec.

3.3. Optical properties

Optical properties of both doped and undoped FCZ samples were investigated. The samples are polished on both sides, and then the sample thicknesses were measured.

3.3.1. Sample preparation for optical properties measurement

FCZ glass samples were first ground in order to achieve parallel surfaces on both the sides.

3.3.1.1. Grinding

A glass plate was used for the grinding process (shown in Figure 3.2). Two types of silicon carbide (SiC) powder were used for the grinding. One was SiC 600 micron powder used for coarse grinding, and the other was SiC 1000 micron powder used for finer grinding.

In the first step, a little amount of SiC 600 micron powder was placed on the glass surface and then mixed with 100% ethanol. The sample was ground slowly in a circular motion to ensure a flat surface was produced on that particular side of the sample. The sample holder was preheated on a Thermolyne HP2305B heater.

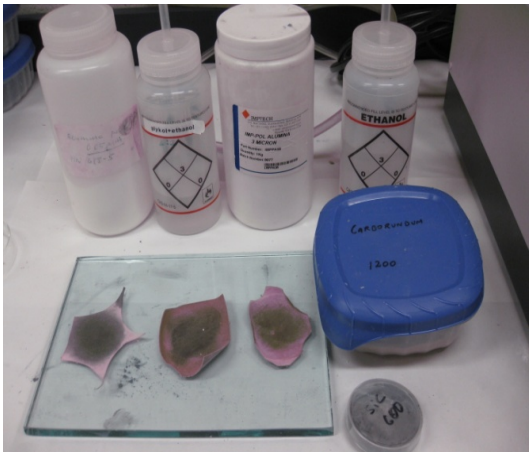

Figure 3.2. The glass plate used for grinding.

Figure 3.3. Thermolyne model HP-2305B hot plate.

Once the holder was hot enough, a little amount of bee wax (yellow in color) was put on the top of the holder and allowed to melt. The sample was carefully positioned on the wax by ensuring the flat surface facing down and the rough surface facing up. The sample holder with the sample on it was then carefully placed in a bowl containing a small amount of water. It was made sure that the sample was not in contact with the water. The bee wax solidified in a few minutes, which helped in holding the sample firmly in place. The sample holder was then taken out of the bowl and dried by a piece of paper napkin. It was then ready for the second stage of grinding. Just like the previous procedure, a small amount of SiC 600 micron powder mixed with 100% ethanol was put on the glass surface. The sample holder with sample was ground slowly in a circular motion until a flat surface was produced. Then, it was washed with 100% ethanol and again was ground with SiC 1000 micron powder in a slow circular motion to ensure a flat sample surface. The process continued until the sample holder with sample could

slide smoothly on the glass surface. After grinding, the sample was ready for the polishing process.

3.3.1.2. Polishing

There are three steps involved in the polishing process.

Step 1: A base was placed in the slot provided by the Buehler Minimet 1000 Polisher machine (shown in Figure 3.4). One or two drops of glycol + ethanol were put on to the polishing cloth of the blue base. The sample holder with previously ground sample was securely held in position on the handle of the polisher. The polishing times and speed modes of the polishing machine were selected. To complete the first stage of polishing, the time was set to 3 to 5 minutes and the speed of rotation was set to 15 to 20 rpm. The polisher machine was then started and it stopped automatically once the process was completed. The sample holder with sample was then cleaned with 100% ethanol and dried with a paper napkin. This step helped in obtaining a shiny surface on the sample.

Step 2: A very little amount of 3 micron alumina (Al_2O_3) powder was put on the polishing cloth in the bowl. A few drops of glycol + ethanol were added on the polishing cloth to act as a lubricant. Just as step 1, the sample holder with the sample was securely held in position on the handle of the polisher. The polishing time was set to 6 to 10 minutes and the speed of the rotation was set to 20 to 25 rpm. The polisher machine was then started and stopped automatically upon the completion of the process. Then the sample was cleaned with 100% ethanol and dried with a piece of paper napkin.

This step helped in obtaining a smoother surface of the sample. The sample was then ready for the third step.

Step 3: A little amount of 0.05 micron alumina mixed with a few drops of glycol + ethanol was placed in a bowl. The rest of the process was same as step 2. The polishing time to complete this step was set to 3 minutes and the speed of rotation was 30 rpm. After this polishing process, the sample was cleaned with 100% ethanol and dried by a piece of paper napkin. This process provided a glossy surface to the sample.

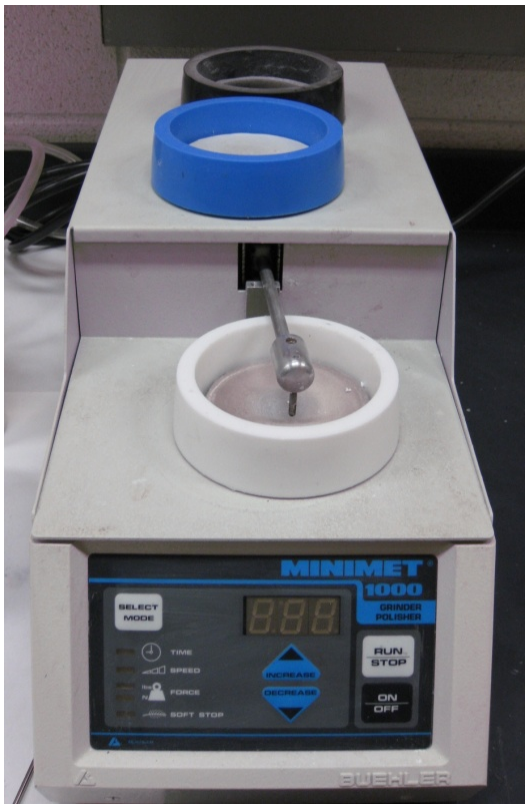

Figure 3.4. MiniMet 1000 grinder-polisher.

The sample holder with shiny sample was put on the Thermolyne HP-2305B hot plate for the bee wax to melt. Once the wax melted, the sample was carefully removed from the holder. It was then flipped and placed back on the holder in such a way that the mirror like surface was facing down. The sample holder with the sample was then cooled down in a bowl containing a small amount of water. The sample was firmly positioned in the solidified bee wax. The entire polishing process was repeated for the other side of the sample. Once all polishing steps were over, the sample holder with the polished sample was placed on the heater in order to melt the bee wax. The sample was then cleaned slowly and carefully with a piece of cotton dipped in diethyl-ether solution. The polished sample was then ready for transmission spectra measurement. Figure 3.5 shows a polished sample of FCZ glass.

Figure 3.5. Typical polished FCZ sample showing nice transparency.

3.3.2. Sample thickness measurement

The thickness of the FCZ glass was measured by an analytical instrument called Fowler Sylvac 50 which is shown in Figure 3.6 [39]. The unit has four components i.e., thickness sensor, stage (platform), handle, and a gauge amplifier. The sample was placed very carefully between the sensor and stage. The sample thickness was read on the display of the gauge amplifier. The accuracy of the measurement was about 0.5 μm [47]. The thickness of Eu doped FCZ glass sample was measured as 0.541 mm and the thickness of the undoped FCZ glass sample was measured as 0.361 mm which was then used for optical measurements.

Figure 3.6. Fowler sylvac 50 – thickness measurement unit.

3.3.3. Transmission spectrum measurement

Transmission spectra in the 500 nm – 3500 nm region were measured by using a Perkin Lambda 900 spectrophotometer. The schematic diagram in Figure 3.7 describes the operation of a spectrophotometer [60]. The operating wavelength range of the

spectrometer was from 185 nm to 3300 nm. These wavelengths were covered by two radiation sources, deuterium lamp and halogen lamp. The halogen lamp covers the wavelengths from 300 nm to 3300 nm and the deuterium lamp covers the wavelengths from 185 nm to 350 nm. The function of the monochromator is to pass the monochromatic light to the sample. The monochromator uses a rotating grating table to pass the monochromatic light through the sample with the help of entrance and exit slits. The transmitted light was then captured by a photomultiplier which operated in the UV to infrared region. The results showing transmittance sprectra obtained by the spectrophotometer are given in relative terms. The transmittance spectra are usually expressed as percentage transmission vs wavelength.

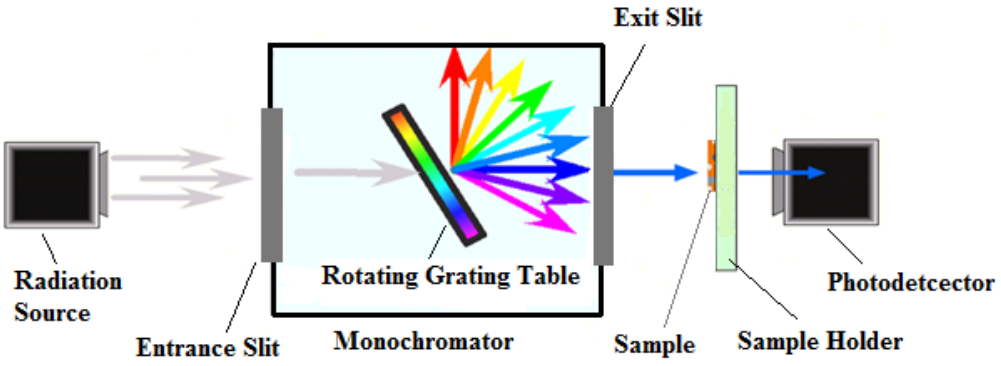

Figure 3.7. Schematic diagram of spectrophotometer.

3.3.4. Photoluminescence (PL)

Steady-state photoluminescence experiments were carried out for FCZ glass samples. In steady state photoluminescence, the emission spectrum obtained is a function of wavelength. The schematic diagram of the experimental setup for steady state photoluminescence is given in Figure 3.8. A halogen-xenon lamp was used to excite the

sample in the UV to the infrared region. The emitted luminescent light was collected by an optical lens and then directed towards an ORIEL cornerstone 1/8 m monochromator. The monochromatic light was converted to an electrical signal by the photodetector attached to the monochromator. The electrical signal obtained was read by the computer. An ORIEL-cooled InGaAs photodiode was used to measure the steady state photoluminescence spectrum.

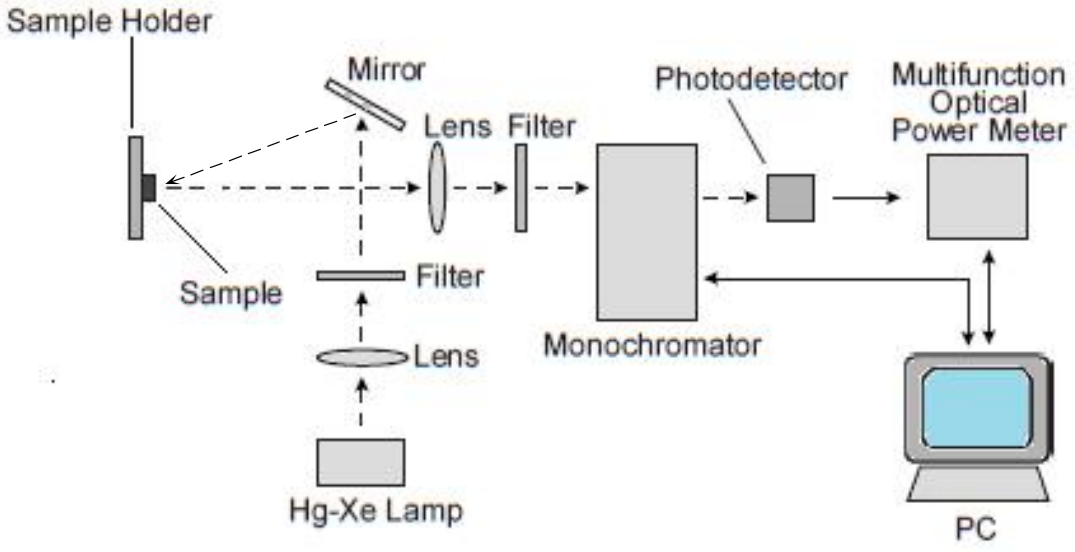

Figure 3.8. Experimental setup for photoluminescence (PL) measurement [38].

3.3.5. Annealing or heat treatment

Annealing plays a very important role in the preparation of FCZ glass samples. Depending on the annealing temperature and time, $BaCl_2$ crystal size and overall structure of the sample can vary significantly. Annealing experiments were done with inert (N_2) atmosphere as well as reducing atmosphere (5% H_2 and 95% Ar). The experimental setup for the annealing process is shown in Figure 3.10. The furnace was

kept at the desired temperature, normally, 250-290 °C. Then annealing gas was supplied into the quartz tube at the rate of 1.0 L/min. The FCZ glass samples were placed carefully in the slots provided in the sample holder. The sample holder was loaded into the quartz tube and sealed. The quartz tube with the sample inside was heated to the desired temperature and time period. The quartz tube was taken out of the furnace and allowed to cool down to the ambient temperature. Finally the samples were taken out of the tube and made ready for measurement. Figure 3.9 shows a schematic diagram for the annealing experimental setup for FCZ glass.

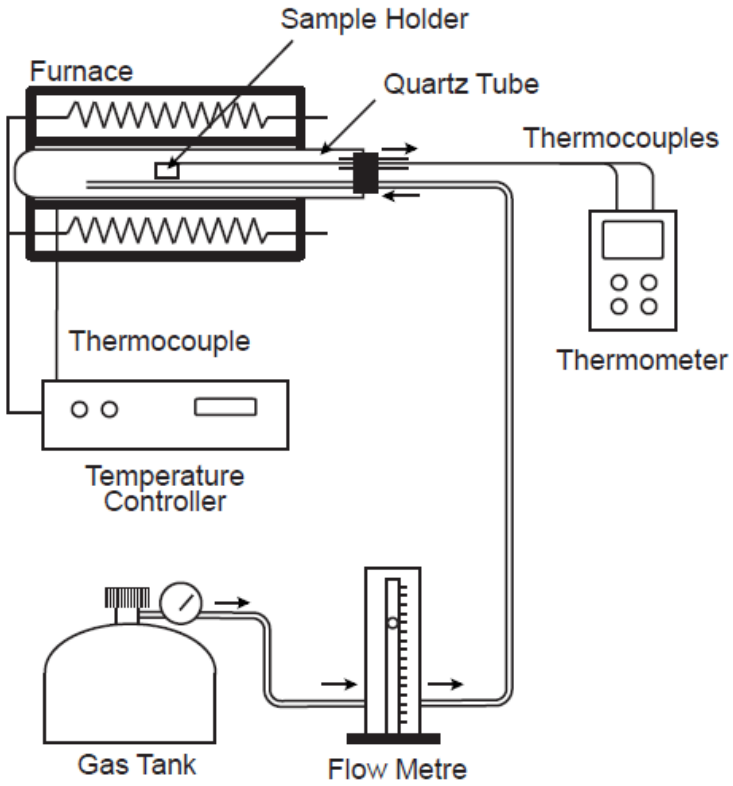

Figure 3.9. Experimental setup of heat treatment / annealing [39].

3.3.6. X-ray luminescence

Figure 3.10 shows the setup used for X-ray luminescence measurements (XL). The GENDEX, GX-1000 dental unit was used as a source for XL measurements. The voltage of the tube was regulated in the range 50-100 kV and the current was set to 10-15 mA. The FCZ glass sample was placed in a PTFE integrating sphere. All the light emitted from the sample was collected in an integrating sphere and then passed to the photo multiplier tube through a PMMA based optical fiber.

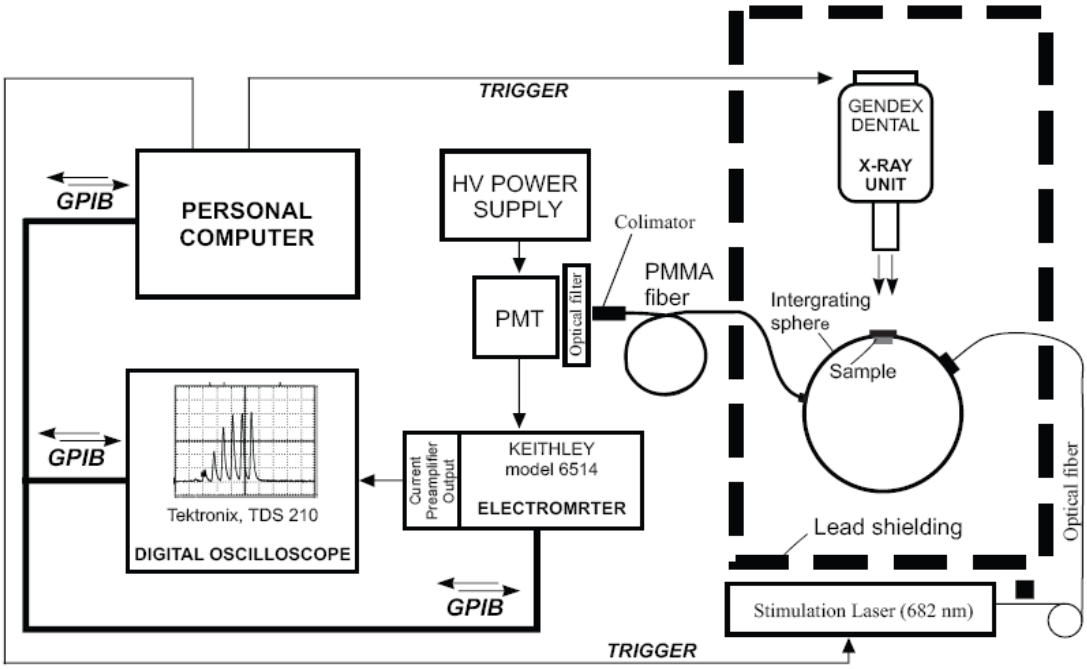

Figure 3.10. Experimental setup for X-ray luminescence measurements [42].

A photomultiplier tube (PMT) was connected to the Keithley 6514 electrometer. The function of the Keithley 6514 electrometer is to measure the current from the PMT. A Keithley 6514 electrometer was connected to a Tektronix TDS 210 digital oscilloscope to measure the "instantaneous" changes in the photocurrent. All the instruments in the experiment, as shown in Figure 3.10, were controlled by a personal computer.

4. RESULTS AND DISCUSSION

The thermal and optical properties of FCZ glasses were investigated using the techniques described in Chapter 3. This chapter not only presents the experimental results and but also discusses the results in terms of various models.

4.1. Thermal properties of doped and undoped FCZ glass

The thermal properties of doped and undoped FCZ glass samples were investigated and compared by carrying out conventional differential scanning calorimeter (DSC) and modulated temperature differential calorimetry (MDSC) experiments. Glass transition, heat capacity and crystallization characteristics of doped and undoped FCZ glasses were investigated to characterize and understand the thermal stability of this glass system

4.1.1. Glass transition and crystallization and phase separation of both doped FCZ and undoped glass samples at different heating rates

An undoped FCZ glass sample with RCl content 14% was studied at the heating rate of 1^{o}C/min. It is observed that crystallization and the glass transition are in the same region. The overlapping of phase transitions in the FCZ sample is clear when the DSC temperature range is increased to 500 ^{o}C which is shown in the Figure 4.1. The values of glass transition temperature, melting temperature, peak crystallization temperature, enthalpy of crystallization and enthalpy of melting are given in table 4.1.

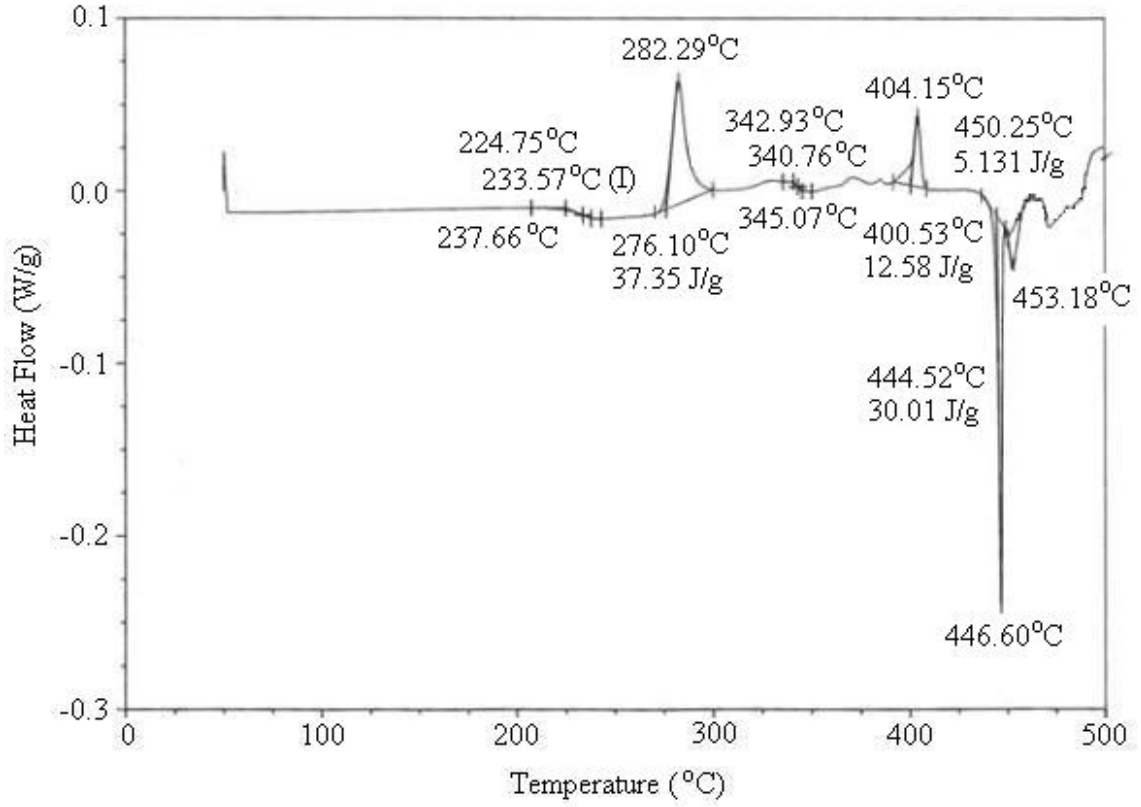

Figure 4.1. Typical DSC thermogram of undoped FCZ glass with relative Cl content of 14% at a heating rate of 1° C/min

Table 4.1. Parameters of undoped FCZ samples obtained at a heating rate of 1° C/ min.

Phases	T_g, °C			T_c, °C		ΔH_c, J/g	T_m, °C	ΔH_m, J/g
	Onset	Inflection	End	Onset	Peak			
1	224.7	233.6	237.6	276.1	282.3	37.3	446.6	30.0
2	340.8	342.9	345.1	400.5	404.1	12.6	453.2	5.1

There is evidence of two different phases in Figure 4.1. For the first phase, T_g is 233.6 °C and the peak crystallization temperature, T_c is 282.3 °C. For the second phase, the T_g-

inflection temperature is 342.9 ^{o}C and the crystallization peak is at 404.2 ^{o}C. The DSC thermogram in Figure 4.1 shows two melting endotherms. The first is at 446.6 ^{o}C and second at 453.2 ^{o}C. The first melting enthalpy is greater than the second melting enthalpy . The overall conclusion is that Figure 4.1 points to the existence of two phases in these glasses.

The FCZ glass sample with R_{Cl} content 14%, doped with Eu^{2+}, was also studied at the heating rate of 1^{o}C/min. Figure 4.2 shows three exothermic peaks, the first two of which are most probably associated with crystallization processes. The first crstallization peak 226 °C is associated with the formation of $BaCl_2$ nanocrystals within the bulk glass, and occurs in the same temperature range as the glass transition in Figure 4.1. The second exothermic peak is most likely associated with the crystallization of the bulk glass. The thirs peak is not discussed in this work and can be due to crystallization or oxidation.

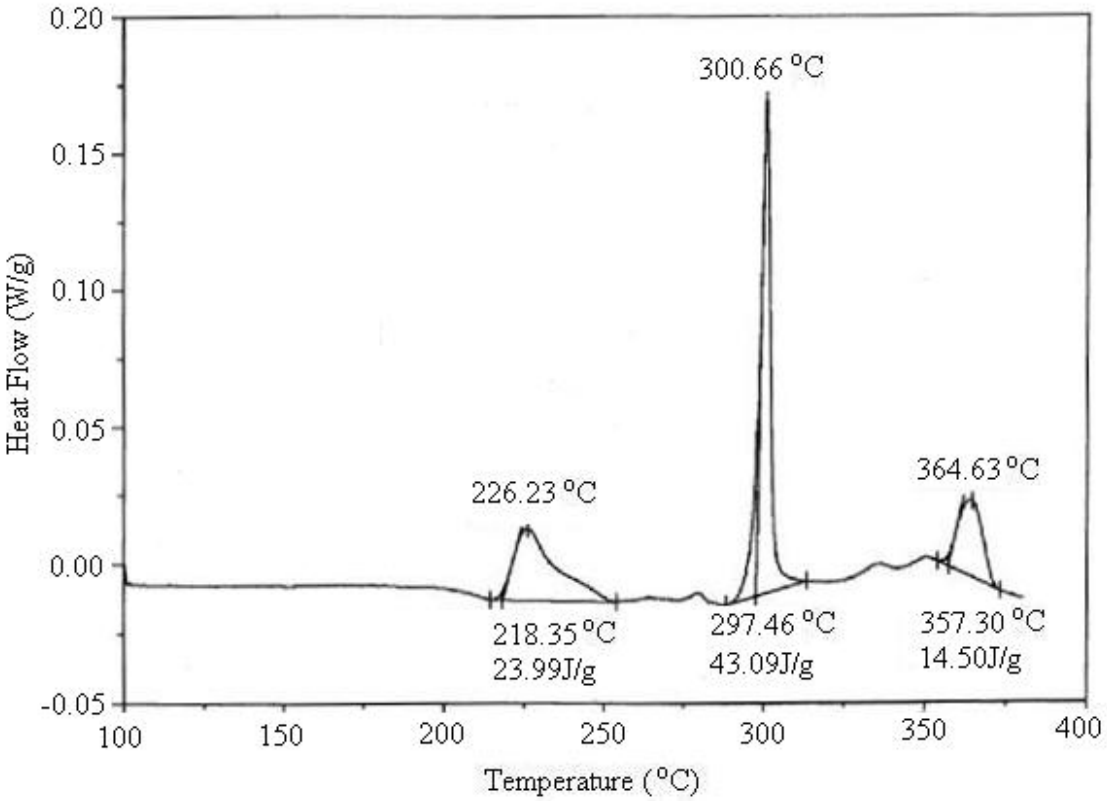

Figure 4.2. A DSC thermogram of a Eu^{2+} doped FCZ glass with relative Cl-content of 14% at a heating rate of 1°C/min.

Various important characteristics of the DSC thermogram of Eu^{2+} doped FCZ glass sample with 14% relative Cl-content at a 1°C/min heating rate has been tabulated in Table 4.2.

Table 4.2. Parameters of Eu^{2+} doped FCZ sample obtained at a heating rate of 1^{o} C/ min

Phases	T_g, ^{0}C	T_c, ^{0}C	ΔH_c, J/g	T_m, ^{o}C	ΔH_m, J/g
	.	Onset	Peak		
1	There may be two transitions present in the same region. MDSC was performed to get a clearer view	218.3	226.2	24.0	Not visible for the particular sample at the given heating rate.
2		297.5	300.7	43.1	
3		357.3	364.6	14.5	

An MDSC scan was used to understand and attempt to separate the overlapping transitions in the 210-220 °C range for Eu^{2+} doped FCZ glass sample. MDSC experiments were conducted at different heating rates to separate the overlapping T_g.; and to get a better resolution and sensitivity for the same sample. MDSC scans of a Eu^{2+} doped FCZ glass sample are shown in Figures 4.3 and 4.4, The result in Figure 4.3 did not have sufficient number of modulations to reveal the transitions clearly. At least four modulations are normally required to reveal a transition. The transition is only at 3 ^{o}C difference that is from 213.8 ^{o}C to 216.5 ^{o}C.

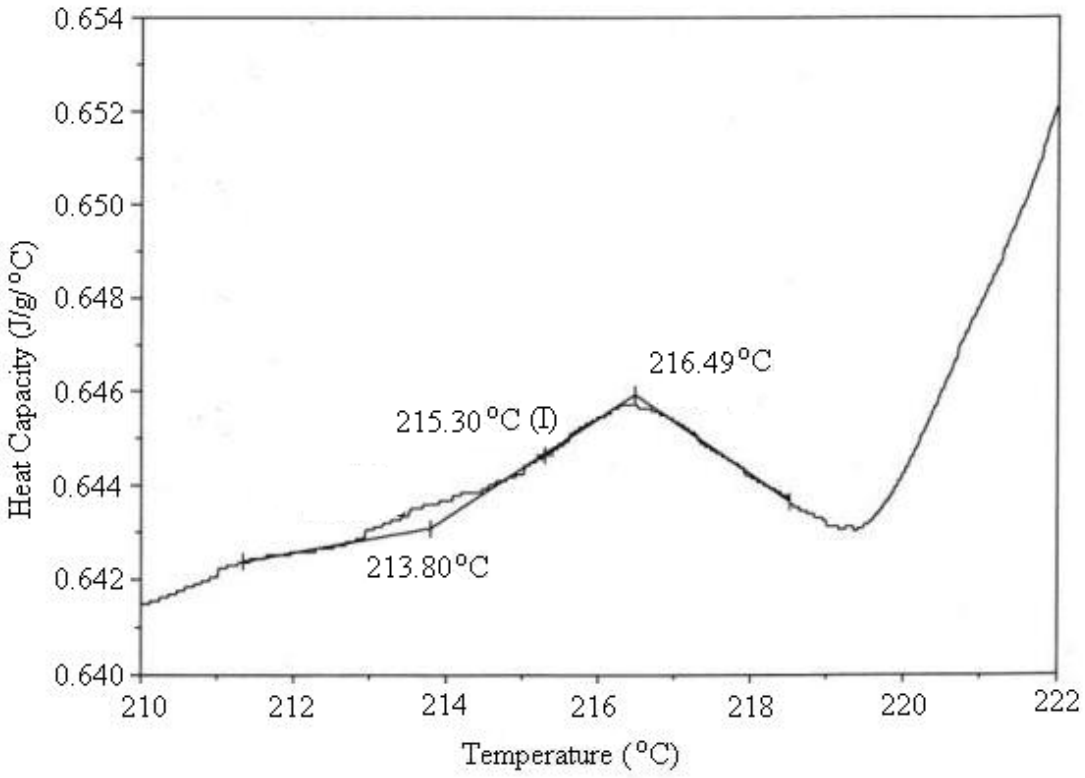

Figure 4.3. MDSC thermogram showing heat capacity vs. temperature plot obtained at 5°C/min for Eu^{2+} doped FCZ glass sample with 14% relative Cl-content.

For better resolution, MDSC was again performed for the same sample at a lower heating rate of 1 °C/min to allow more modulations over the temperature range of interest. The heating schedules consisted of a heating scan starting from a temperature of 20 °C to 380 °C, at different heating rates and heating periods in MDSC. Thermal analysis software of TA Instrument was used to calculate the specific heat capacity from the reversing heat flow. The values of the heat capacity (C_p) and glass transition temperature (T_g) were established from a step transition of the heat capacity in the glass transition region as illustrated in Figure 4.4. As apparent from Figure 4.4, the reversing heat flow v temperature scan result shows a clear step transition of the heat capacity curve; and only one T_g at the inflection point, which is 239.1 °C.

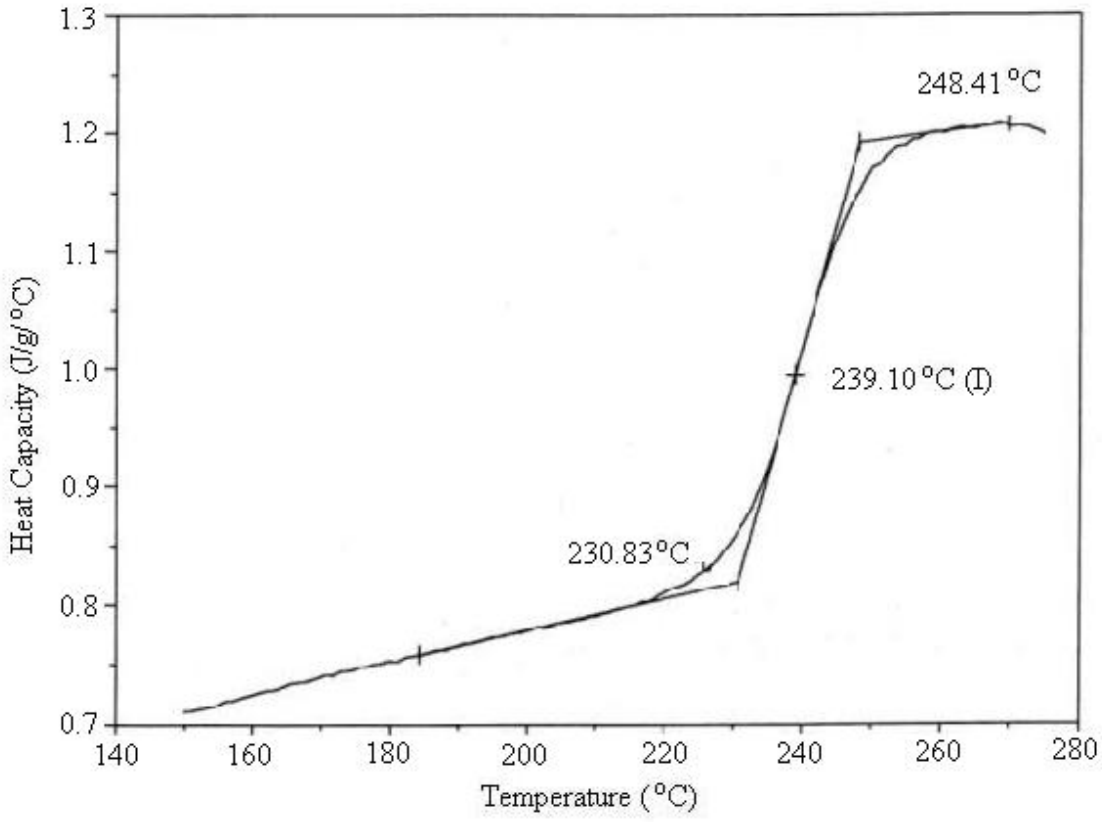

Figure 4.4. Typical MDSC thermogram of the FCZ glass sample during a heating scan at 1° C/min. The measured T_g is taken to be at the inflection point, that is, 239.1 °C.

4.1.2. Glass transition and phase separation of Sm-doped FCZ glasses

Figure 4.5 shows various DSC heating scans for FCZ samples for different amounts of relative chlorine (Cl) content (R_{Cl}); all doped with 0.2% SmF_3. The doped FCZ glasses with 5% and 7% relative Cl addition (R_{Cl} = 0.05 and 0.07) are characterized with one single wide crystallization exothermic peak in the temperature range up to 320 °C. It is clear from Figure 4.5 that there are significant structural changes related to the halogens (Cl and F) content. It is also observed that the sample corresponding to R_{Cl} = 5% and 7%, the glass transition is in the region of 230-250 °C.

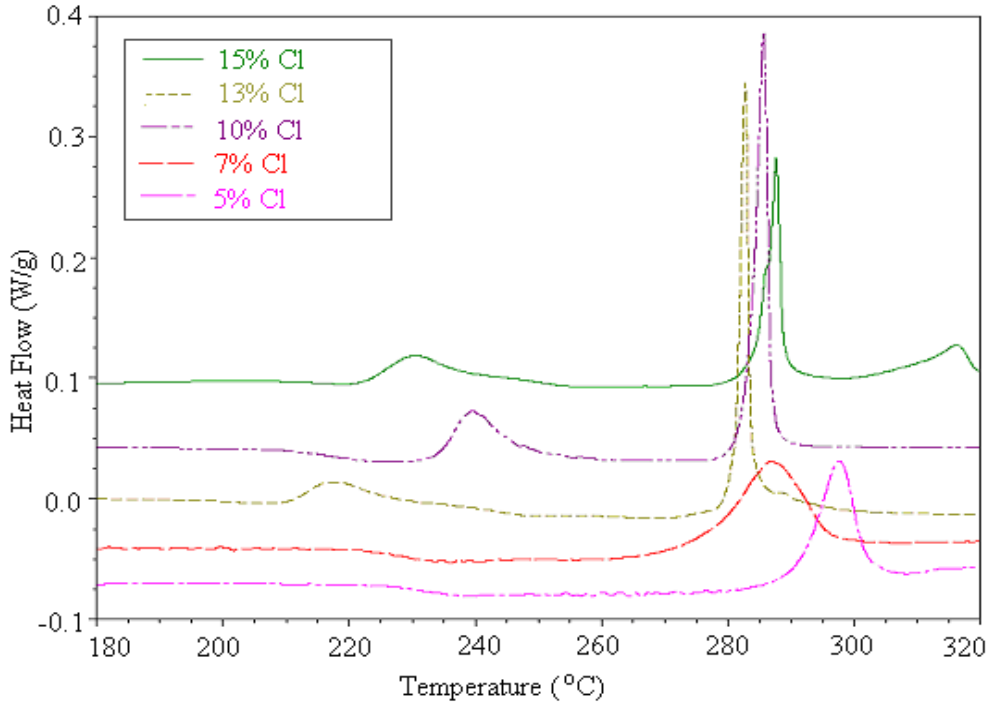

Figure 4.5. DSC scan of 0.2 % Sm^{3+} doped FCZ glasses with different amounts of relative Cl, that is Cl/(Cl+F). Relative Cl amounts were 5%, 7%, 10%, 13% and 15%. The DSC scans illustrate the transition from one to two phases.

It is also observed that the samples corresponding to R_{Cl} = 10%, 13% and 15%, show two crystallization peaks. The first peak, as discussd above, is due to the crystallization of $BaCl_2$ crystals in the glass structure. The glass transition events in these glasses are obscured by the crystallization phenomena. To obtain a clear view of glass transition and phase separation for the same samples, MDSC experiments were performed, the results for which are shown in Figure 4.6. Figure 4.6 shows MDSC thermograms for R_{Cl} = 5%, 7%, 10%, 13% and 15%, 0.2% Sm^{3+} doped FCZ glasses for which C_p is shown as a function of the sample temperature. For the sample R_{Cl} = 5%, which is shown as the bottom curve, there is only one glass transition (T_g at 242.5 °C). For the sample R_{Cl} = 15%, which is shown as the top curve, one can clearly identify two sigmoidal-type step

changes in C_p, one at a lower temperature (T_g at 210.9 °C), and the other at a higher temperature (T_g at 251.6 °C).

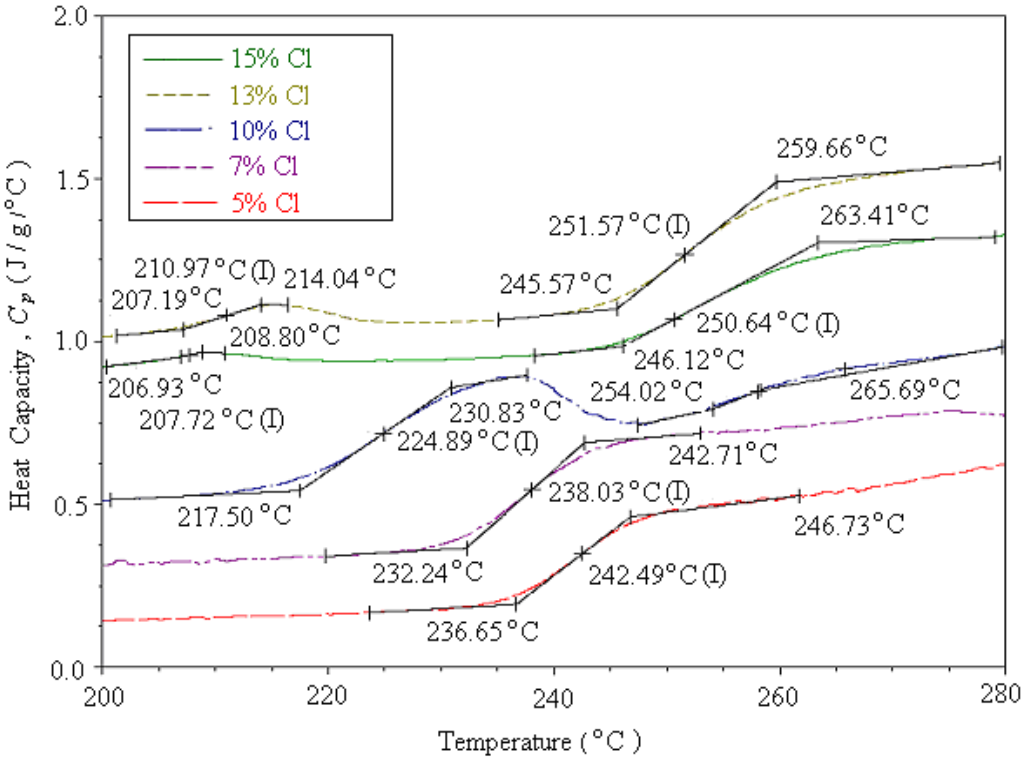

Figure 4.6. MDSC heat capacity curves of 0.2% Sm^{3+} doped FCZ glasses with halogen dependence, showing T_g of different glass phases. The halogen content is shown as relative Cl content, that is, Cl/(Cl+F)

Glasses with R_{Cl} = 10 and 15% also show similar behaviour. The observation of two possible glass transitions indicates the presence of two phases in these glasses with higher R_{Cl}. Similar MDSC thermograms have been used to identify different phases in other glasses [46]. Hendy and Edgar, 2006; Edgar *et. al.,* 2006 have proposed that the FCZ glasses can be phase separated for these compositions [24], [30]. The DSC thermograms for EuF_2 doped FCZ glasses are similar [3].

4.1.3. Glass transition, crystallization and C_p dependence of both phases of Sm^{3+} and Eu^{2+} doped FCZ glass samples on the amount of doping materials and halogen contents

The dependence of the crystallization temperature, T_c, on the Cl-content is shown in Figure 4.7. The crystallization temperature of the bulk glass initially decreased with the R_{Cl} content and then remained constant in the two-phase region, whereas the crystallization of the $BaCl_2$ phase decreased with R_{Cl} content. Figures 4.7 and 4.8 are useful in choosing the annealing temperature for the formation of nanocrystals.

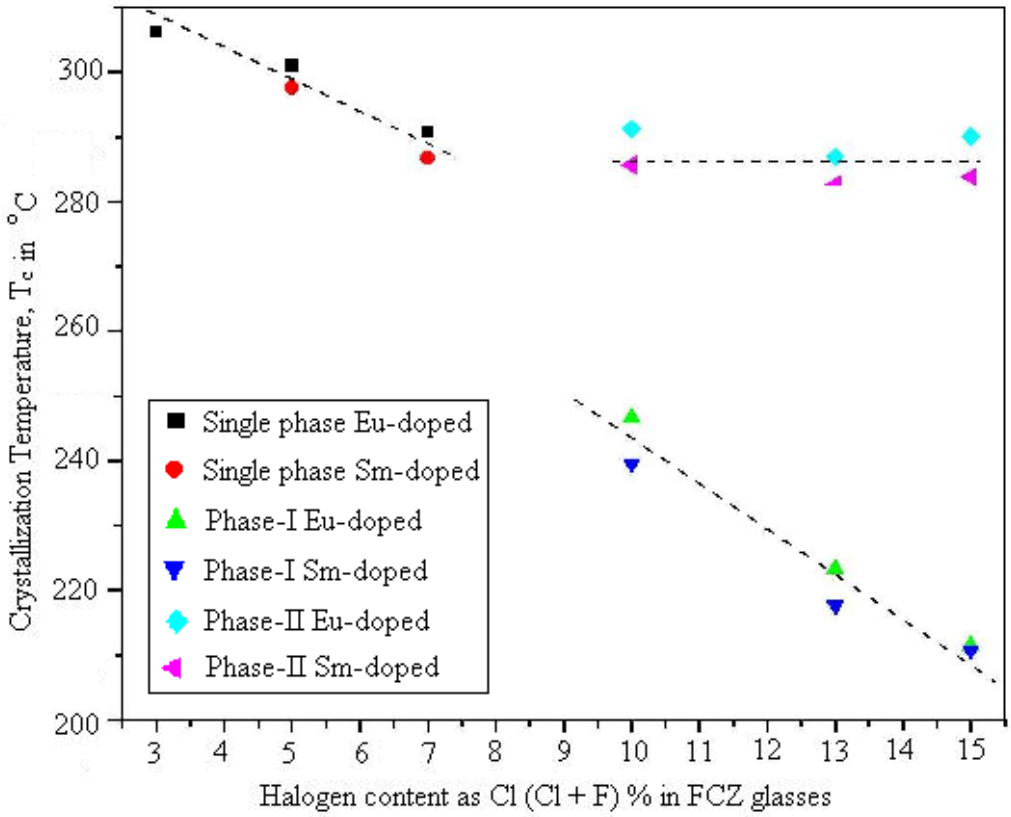

Figure 4.7. Crystallization temperatures, T_c dependence on halogen content in Sm^{3+} and Eu^{2+} doped FCZ glass samples.

Figure 4.8 shows the dependence of the crystallization temperature (T_c) on the concentration of rare-earth dopants for both Sm^{3+} and Eu^{2+} doped FCZ glass samples. There is only a small increase in the crystallization temperature of phase-II with the dopant concentration. It is observed that most of the changes of crystallization temperatures are related to the lower temperature crystallization phase, that is, phase-I. This is a sign that rare earth (RE) dopants were predominantly entering the first phase during alloy preparation. The higher temperature phase, phase-II, changed only slightly. Based on the above results, annealing temperatures were selected, that is between two glass crystallization phases, at 250 ^{o}C [13]. The annealing times and annealing atmosphere (nitrogen or hydrogen) were varied in order to crystallize phase-I only and to keep phase-II unchanged in order to form small nanocrystals within a glass matrix to obtain a glass-ceramic sample, which leads to an increases XL efficiency, while keeping the glass almost transparent [3].

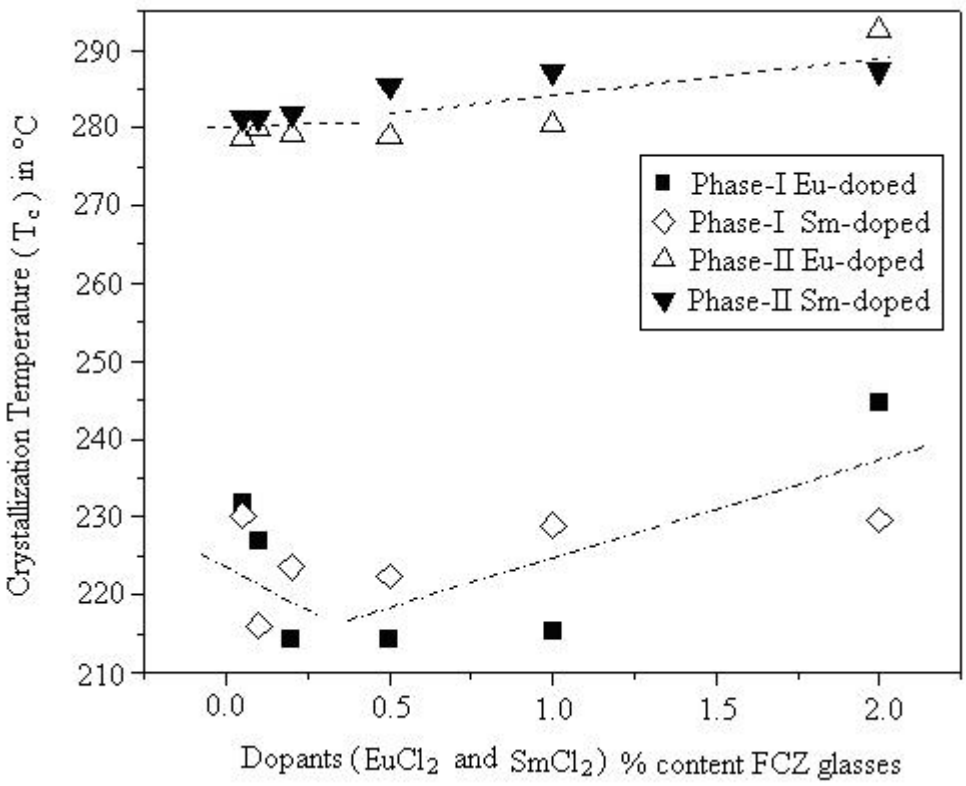

Figure 4.8. Crystallization temperatures, T_c of phase-I and phase-II of FCZ glass samples doped with different amounts of $EuCl_2$ and $SmCl_3$.

4.1.4. Heat capacity (C_p) dependence on the halogen contents of both Sm^{3+} and Eu^{2+} doped FCZ glass samples

Figure 4.9 and 4.10 show the dependence of the heat capacity on the halogen contents of Sm^{3+} and Eu^{2+} doped FCZ glass samples, respectively. From Figure 4.9 and Figure 4.10, it is clear that the heat capacity values increase with increasing halogen content in both Sm^{3+} and Eu^{2+} doped FCZ glass samples. Heat capacity values were evaluated at two different fixed temperatures, that is 50 ^{o}C and 150 ^{o}C. Glass heat capacities of the samples were measured by using the MDSC at the heating rate of 1 ^{o}K/min and with a modulation amplitude of ± 1 ^{o}C and with modulation period of 60 seconds.

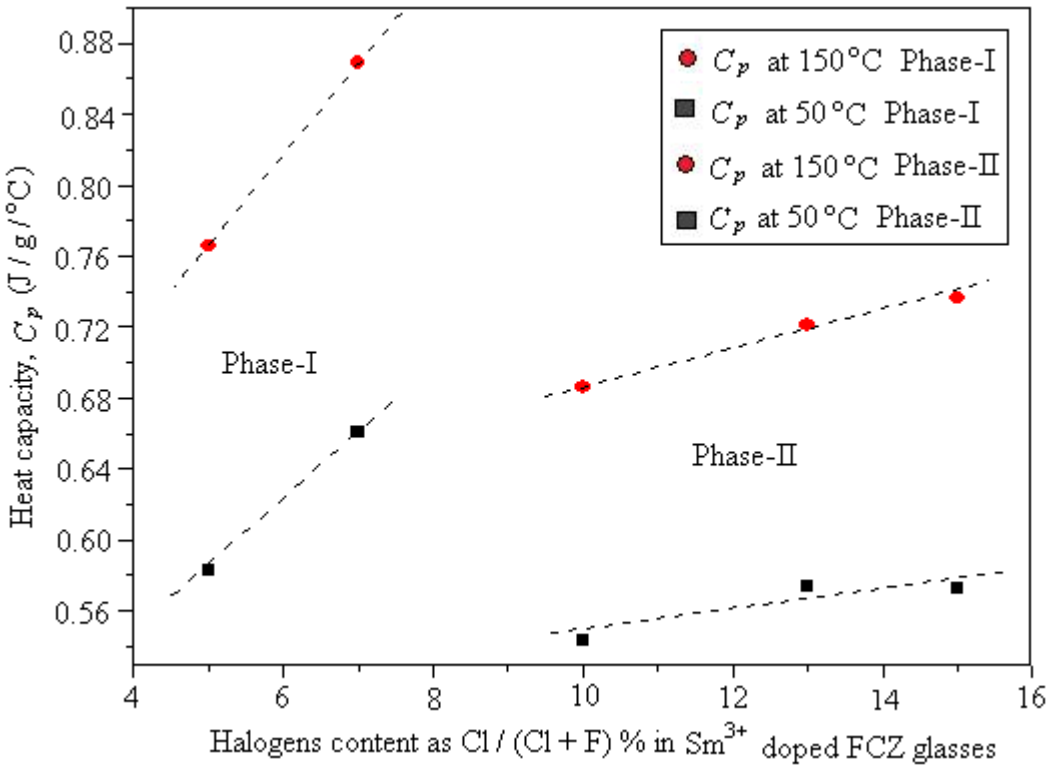

Figure 4.9. Heat capacity, C_p dependence on halogens Cl (Cl+F) % content in Sm^{3+} doped FCZ glass sample.

4.1.5. Kissinger plots to get the activation energy of doped and undoped FCZ glass samples

As discussed in the crystallization kinetics section of chapter 2, the analysis of non-isothermal crystallization kinetics by using DSC scans gives the activation energy for the crystallization process. Multiple DSC scans were taken and the shift in the crystallization peak temperature T_p was examined since T_p shifts with the heating rate r and the shift depends on the activation energy. The T_p-r data were then plotted as a Kissinger plot according to ln (r/T_p^2) vs. $1/T_p$. The slope of the best line to the Kissinger plot should give the activation energy, E_A, for the crystallization process.

The fundamental equation describing the relation between extended volume fractions and crystallized volume fractions is given as [48].

$$dx = (1 - x)\, dV_{\text{ex}} \tag{4.1}$$

Where, V_{ex} is the extended volume fraction and x is the crystallized volume fraction.

The above equation can be rewritten in terms of rates as [48]:

$$\dot{x} = (1 - x)\dot{V}_{\text{ext}} \tag{4.2}$$

For heterogenous nucleation, a Kissinger technique is described by using the equation [32]:

$$\ln(r / T_p^2) = -E_A/kT_p + C_K + \ln[f_1(x_c)] \tag{4.3}$$

Where, r is the heating rate, T_p is the peak crystallization temperature, C_K is a constant which depends on activation energy, E_A, but not on the heating rate or peak crystallization temperature. As mentioned by Kasap and Juhasz [48], the term $f_1(x_c)$ is a function of the total crystallized volume fraction, x_c at T_p. Also, ln $[f_1(x_c)]$ changes very slowly with T_p, therefore, the slope of the Kissinger plot gives activation energy, E_A. According to Kasap and Juhasz [48], the crystallized volume fraction, x_c is relatively independent of heating rate or is approximately 0.632. The equation is rewritten as [6], [48]:

$$\ln(r/T_p^2) = -E_A/kT_p + C \tag{4.4}$$

where, C is a constant.

It is apparent that the best line fit to the plot of $\ln(r/T_p^2)$ vs $1/T_p$ should give the apparent actication energy E_A. The apparent activation energies were measured by using the peak rate temperature shift method in the DSC mode at various heating rates corresponding to 0.5, 1, 2, 5, 10 and 20 ^oC/minute. It is observed that the activation energies obtained from $\ln (r / T_p^2)$ vs. $1 / T_p$ plot are different for both the doped and undoped FCZ glass samples. Peak crystallization temperatures, heating rates and $\ln (r / T_p^2)$ used in the Kissinger plot are summarized in Table 4.3 and Table 4.4. In Table 4.3 and 4.4, T_{max}, represents peak crystallization temperature, T_p .

Table 4.3. Data collected for Kissinger plots of undoped FCZ glass samples under different heating rates.

r in ^oC/min	T_{max} in ^oC	T_{max} in K	$1 / T_{max}$ in K^{-1}	$\ln (r/T_{max}^2)$
0.5	295.44	568.44	0.001759	-13.38
1	300.66	573.66	0.001743	-12.70
2	306.46	579.46	0.001726	-12.03
5	315.73	588.73	0.001699	-11.15
10	323.54	596.54	0.001676	-10.48
20	333.32	606.32	0.001649	-9.82

Figure 4.10 shows a Kissinger plot for an undoped FCZ glass sample whose activation energy E_A was computed by using equation 4.4, and is equal to 269.1 kJ/mole.

Table 4.4. Data collected for Kissinger plots of 0.2 % Eu-doped FCZ glass samples under different heating rates.

r in ^{o}C/min	T_{max} in ^{o}C	T_{max} in K	1 / T_{max} in K^{-1}	ln (r/T_{max}^{2})
0.5	274.69	547.69	0.001826	547.69
1	281.91	554.91	0.001802	554.91
2	292.73	565.73	0.001768	565.73
5	306.65	579.65	0.001726	579.65
10	320.06	593.06	0.001686	593.06
20	337.37	610.37	0.001638	610.37
40	346.27	619.27	0.001615	619.27

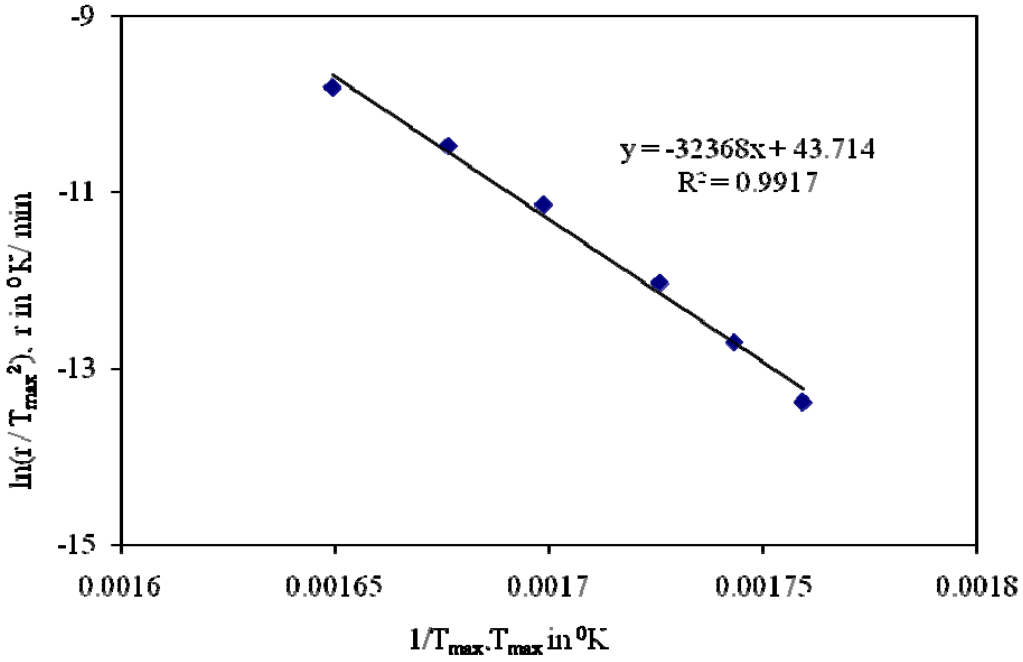

Figure 4.10. Kissinger plot for undoped FCZ glass samples with different heating rates and the calculated activation energy is 269.1 kJ/mole.

Figure 4.11 shows a Kissinger plot for a 0.2% Eu^{2+} doped FCZ glass sample whose activation energy, E_A was computed by using equation 4.4 and is equal to 289.9 kJ/mole.

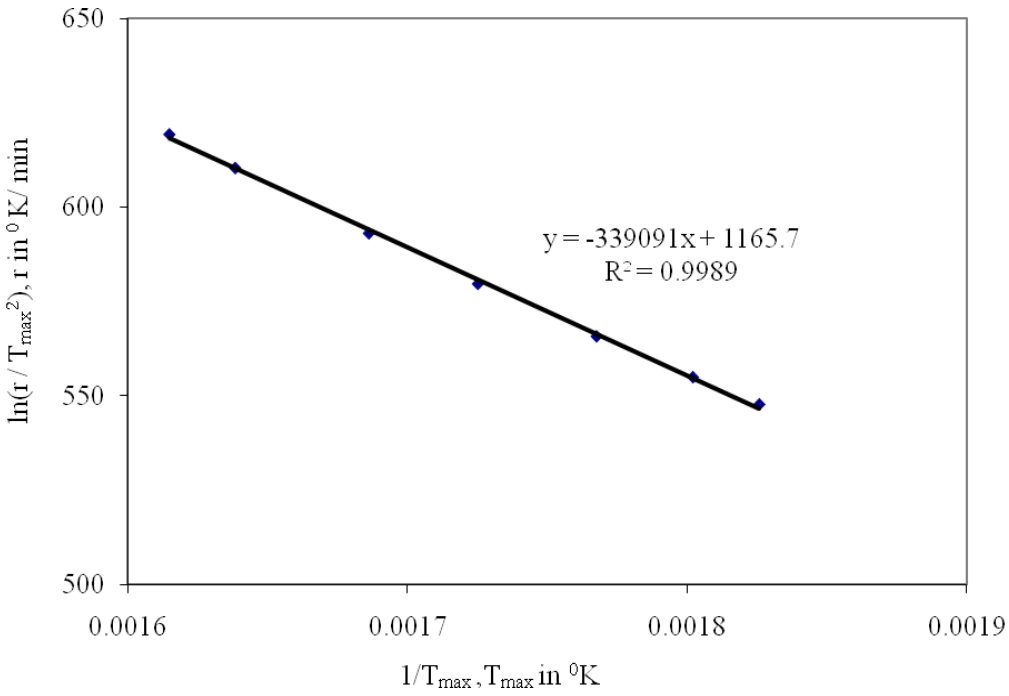

Figure 4.11. Kissinger plot for of 0.2 % Eu-doped FCZ glass sample with different heating rates and the activation energy is 289.9. kJ/mole.

Kissinger plots in Figure 4.10 and Figure 4.11 for both doped and undoped FCZ glass samples show that doping leads to a slight increase in the activation energy. It can be said that the doped FCZ glass sample having higher activation energy is more thermally more stable than the undoped FCZ glass sample.

4.2. Optical properties of FCZ glass samples

In this section optical properties of doped and undoped FCZ glass samples are investigated. Transmission spectra of both doped and undoped glass samples have been measured and optical bandgaps corresponding to an absorption coefficient 10^3 cm^{-1} have

been determined. The behavior of FCZ glasses annealed in N_2 and H_2 gas atmospheres, X-ray and photoluminescence (XL and PL) properties of FCZ glasses were also studied in this section. It was assumed that the FCZ glass compositions can be used as a host to dope with rare earth elements; however there is a strong dependence of glass transparency on the composition, which was taken into account while conducting the experiments.

4.2.1. Transmission spectra of doped and undoped FCZ glass samples

Transmission spectra of both 0.2 % Eu-doped and undoped FCZ glass samples were calculated by using the transmittance equation which is described by Munzar *et al*, 2006 [49], and it is given as:

$$T_{cal}(\lambda)=\{[1-R(\lambda)-r]^2\exp[-\alpha(\lambda)+S(\lambda)d]\}/\{[1-R(\lambda)-r]^2)\exp[-2\alpha(\lambda)+S(\lambda)]d]\} \quad (4.5)$$

$$R(\lambda) = [1-n(\lambda)]/[1+n(\lambda)] \quad (4.6)$$

where, R is the reflection coefficient, $n(\lambda)$ is the refractive index, $\alpha(\lambda)$ is the absorption coefficient, d is the thickness, r represents possible losses due to surface micro defects, $S(\lambda)$ is the light scattering. This method is described in Munzar *et al*, 2006 [49].

Figure 4.12 shows the transmission spectrum of a 0.2%Eu doped FCZ glass. The 0.2 % Eu doped FCZ glass has been found to be more transparent than the undoped FCZ glass sample. The refractive indices of the glass samples were calculated by using interpolation based on an optimal polynomial method.

The absorption coefficient was fitted by using Urbach rule [49]:

$$\alpha(\lambda) = \alpha_{o} \exp(h\nu/\Delta E) = (10^{3}\text{cm}^{-1}) \exp[(h\nu - E_g^{03}) / \Delta E] \quad (4.7)$$

Where, $h\nu$ is the photon energy, ΔE is Urbach tail parameter, α_0 is a constant and E_g^{03} is the adjustable parameter which may be identified as optical band gap corresponding to an absorption coefficient 10^3 cm^{-1} in undoped materials and some effective bad gap like parameter characterizing the optical absorption of Eu^{2+} ions in doped CGZ glasses . The adjustable parameters $\alpha_{0,}\Delta E$ and r are used in equation (4.5) to fit $T_{exp}(\lambda)$ as closely as possible to the experimental data. Figure 4.13 shows the experimental transmission spectrum of a doped FCZ sample and the calculated spectrum.

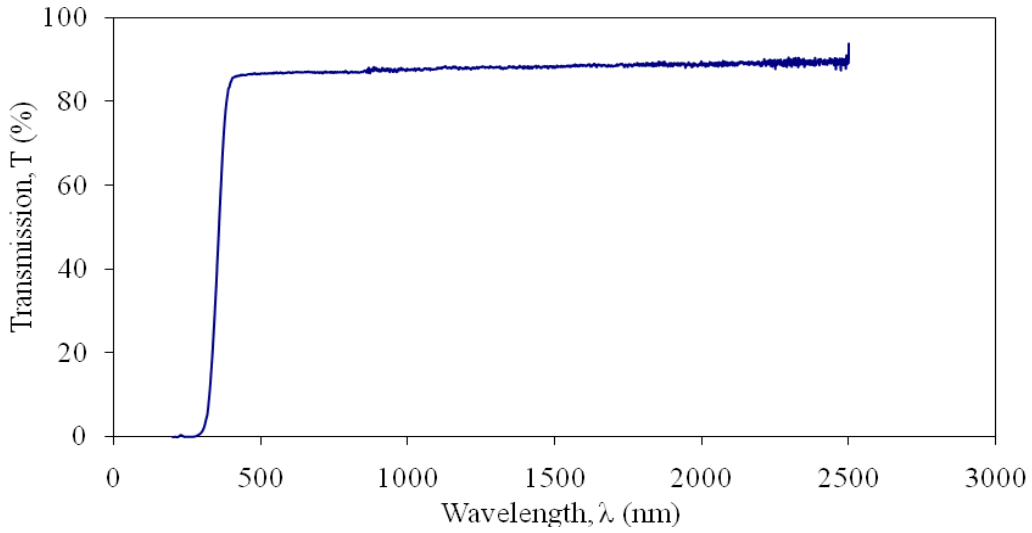

Figure 4.12. Transmission spectra of 0.2 % Eu-doped FCZ glass samples.

As shown in Figure 4.13 it is clear that fit to data from Equation (4.5) is relatively good. The absorption has been calculated by minimizing the difference between $T_{cal}(\lambda)$ and $T_{exp}(\lambda)$ where the latter is the experimental spectrum. The parameter, E_g (estimated from

10^3 cm^{-1}) determined from this work is 3.65 eV for 0.2 % Eu doped and 6.05 eV for undoped FCZ glass samples, the former is consistent with the intense optical absorption by Eu^{2+} ions in UV region below 350 nm.

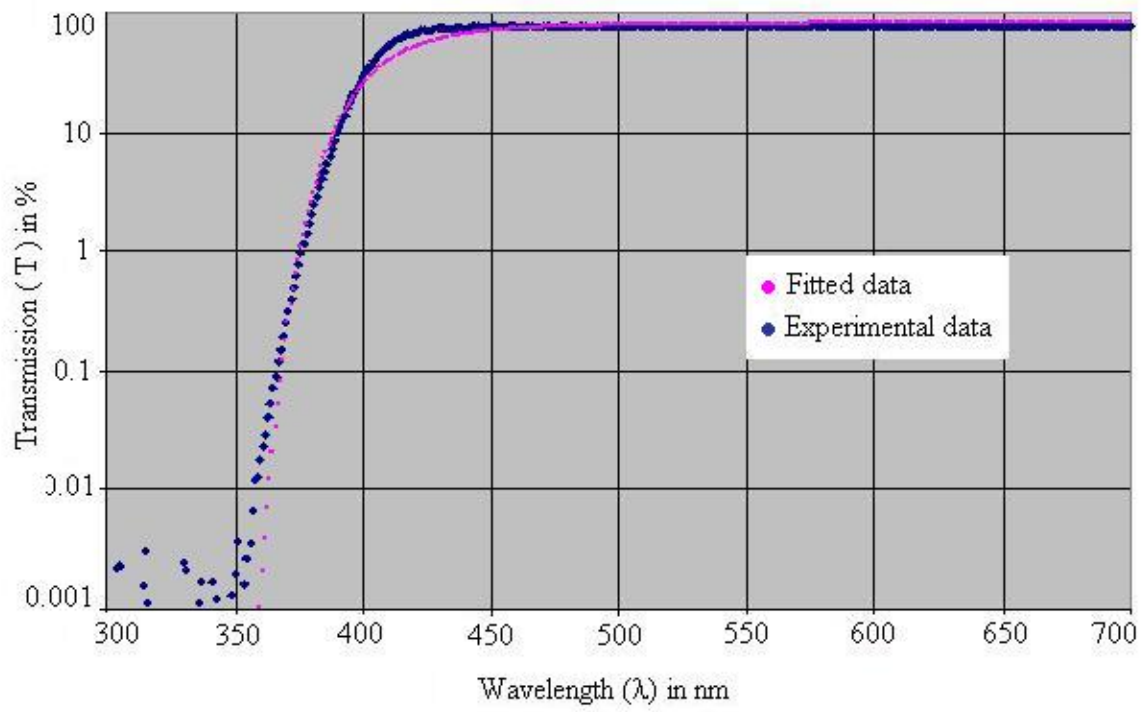

Figure 4.13. Comparison of fitted data and experimental data. The calculated transmission and experimentally measured transmission overlap each other.

The graphical procedure of E_g determination is illustrated by Figure 4.14. It is worth remembering here that the Eu doped FCZ glass is more thermally stable than undoped one. It also preserves high optical transparency in the visible and IR region. Therefore it may be used as an effective host for co-doping with another rare earth in the manufacturing of optical components.

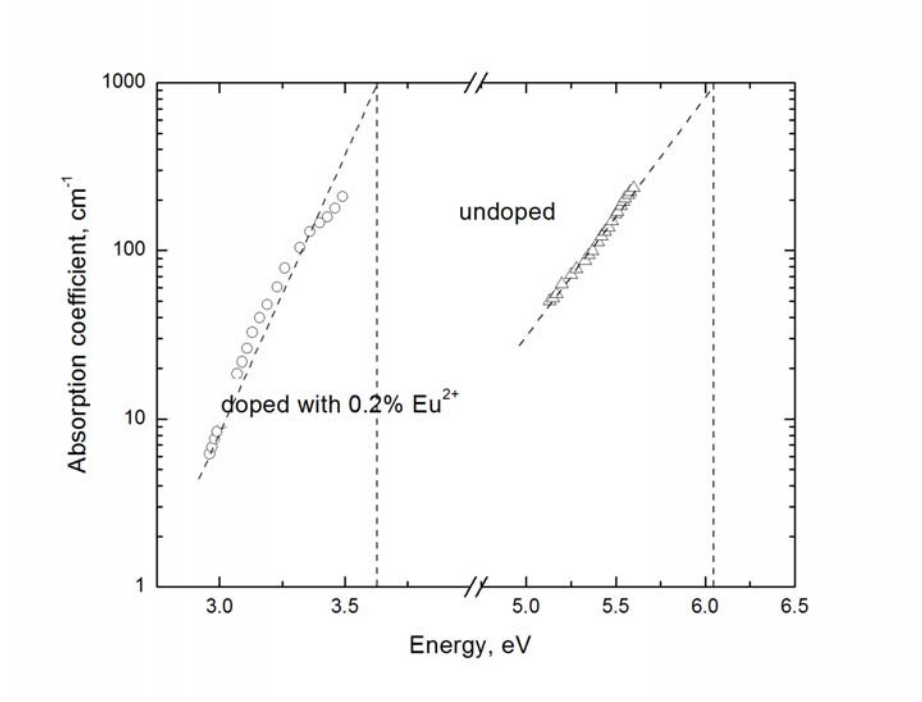

Figure 4.14. Absorption spectra of both 0.2 % Eu doped and undoped FCZ glass samples.

4.2.2. Luminescence properties of FCZ glass samples

Eu-doped FCZ glasses have been extensively studied by Edgar *et al.,* 2005, 2003 and Schweizer *et al.,* 2003 [27], [51], [52]. Further experiments and analysis were concentrated on Sm doped FCZ glass samples.

4.2.2.1. X-ray induced luminescence (XL)

The X-ray luminescence of Sm-doped FCZ was investigated as a function of the Sm-content (C_{Sm}). Figure 4.15 shows the dependence of the XL yield on the Sm-content.

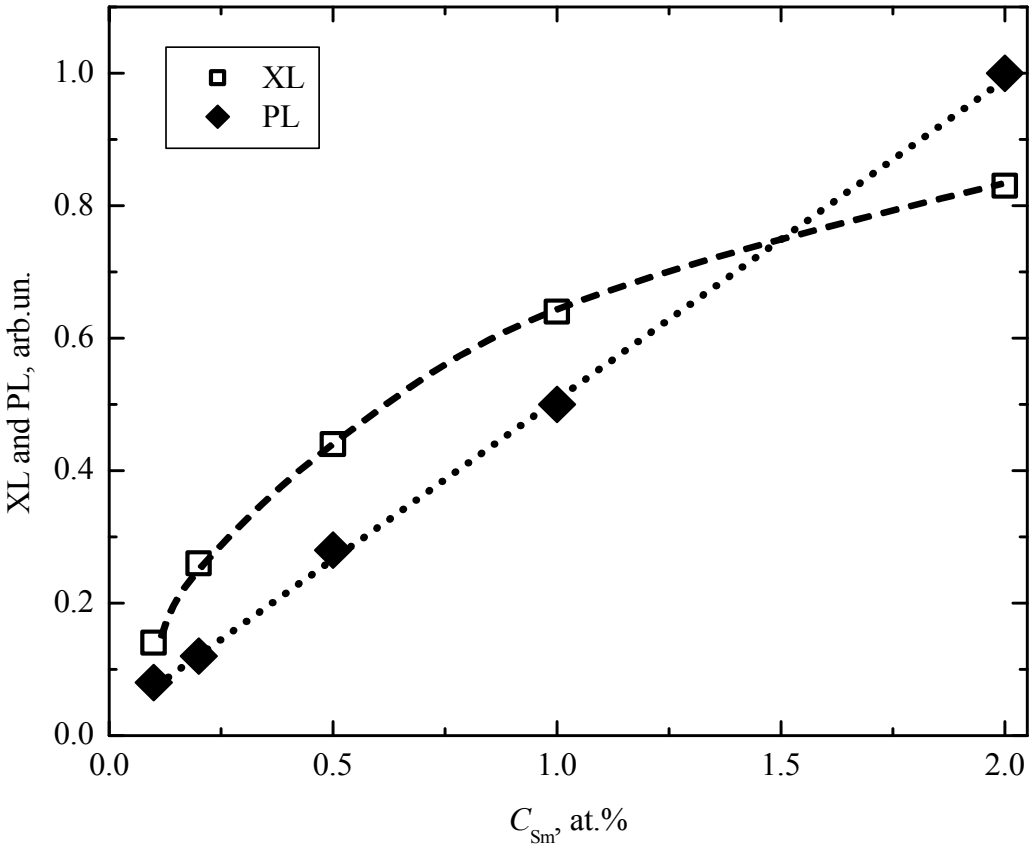

Figure 4.15. X-ray luminescence and photoluminescence intensity versus the concentration of Sm (C_{Sm}). The PL linearly depends on C_{Sm}, while the XL clearly demonstrates a sub linear dependence.

Figure 4.15 shows the dependence of X-ray luminescence and photoluminescence (PL) of Sm-doped FCZ with 13% relative Cl content on the C_{Sm}. It can be seen that the PL increases linearly with the Sm-concentration (C_{Sm}). The difference between the two results is due to the different nature of the excitation process involved in the PL and XL.

Figure 4.16 shows the comparison of photoluminescence (PL) and x-ray luminescence (XL) spectra of Sm^{3+} doped FCZ glasses. The emissions have been attributed to Sm^{3+} ions. The spectra are almost identical in the range of 550 – 750 nm, while there are

differences in the dependence of the integrated intensity of PL and XL on the partial Cl-content.

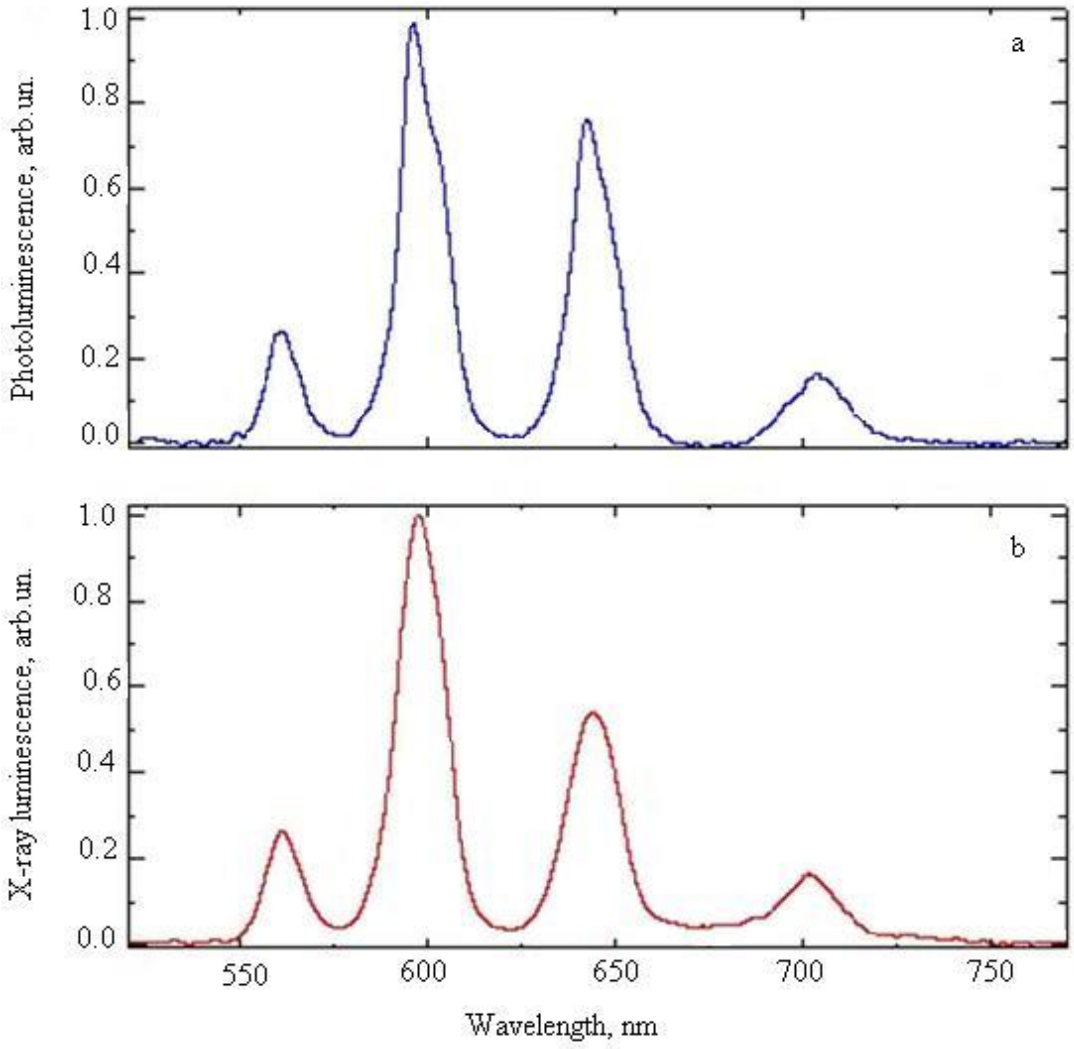

Figure 4.16. Comparison of (a) photoluminescence, PL and (b) X-ray luminescence, XL spectra of Sm^{3+} ions embedded in FCZ glasses.

The partial amount of Cl is defined as the ratio of the Cl-concentration C_{Cl} to the overall concentration of halogens, i.e. $R_{Cl} = C_{Cl} / (C_{Cl} + C_F)$. In thermal analysis (DSC and MDSC) section of this chapter (Figure 4.7), the formation of two phases was occurring

in FCZ glasses when the R_{Cl} content was 10% or higher. Hence, it is clear that, R_{Cl} contents not only affects thermal properties as observed in DSC (heat flow) and MDSC (heat capacity) but also affects XL and the PL properties of the sample materials studied, which is evident in Figure 4.17.

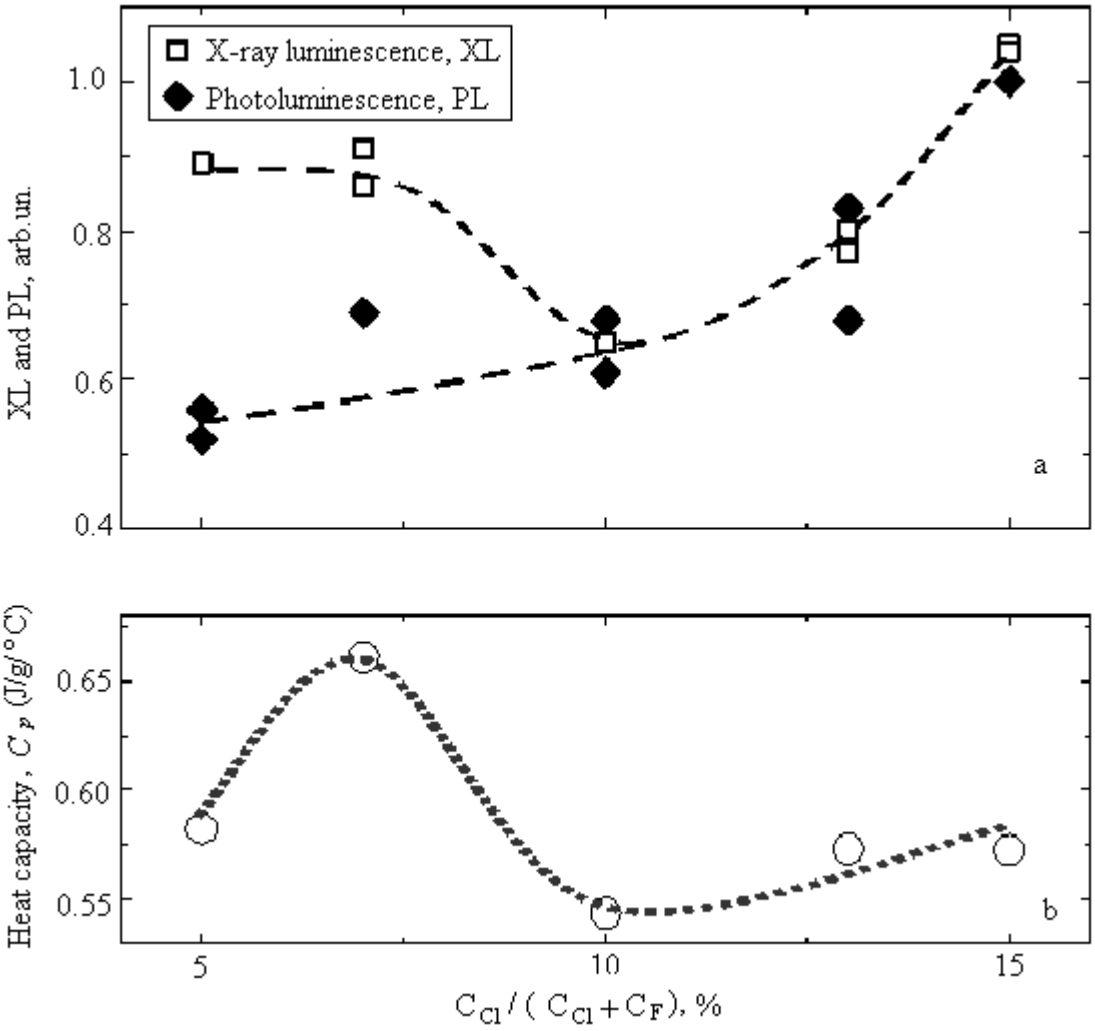

Figure 4.17. (a) X-ray luminescence (XL) and Photoluminescence (PL) intensity versus partial content of Cl; (b) Heat capacity versus partial content of Cl.

Figure 4.17 (a) indicates a good correlation between the XL and C_p dependences on the R_{Cl} concentration while the PL monotonously increases with higher R_{Cl} concentration.

XL excitation first involves the generation of an energetic primary electron through the photoelectric effect. The primary electron generates many electron-hole pairs by ionization of the FCZ glass which then has to diffuse in the glass matrix to the dopant centers where they can recombine through Sm^{3+} levels. Thus, the XL excitation depends strongly on the structure of the FCZ glass. Therefore, the correlation between both XL and C_p is not unexpected since both depend on the FCZ glass structure. Figure 4.17 (b) shows the dependence of heat capacity (C_p) on the partial Cl-content (R_{Cl}) to support the change in the structure of FCZ glasses above a R_{Cl} content of 10%.

4.2.2.2. The influence of annealing on photoluminescence and X-ray luminescence

It is well known that annealing plays a very important role in the preparation of FCZ glass-ceramic materials [44], [50], [53]. Experiments were conducted to determine how the X-ray luminescence signals changes under different annealing conditions. Experiments were performed in an inert (N_2) atmosphere as well as in a reducing atmosphere (5% H_2, 95% Ar). Annealing has been initially tested at a temperature of 250 °C. The duration of the annealing was set to 30 min. It is observed that any annealing process significantly increases the magnitude of the XL signal compared to the one observed in the corresponding unannealed glass sample. Most of the annealed samples in an inert atmosphere become white and non transparent at the annealing temperatures that were used. However, the samples annealed at 250 °C in a reducing atmosphere remain transparent.

Figure 4.18 shows DSC scans on unannealed and annealed samples. It is clear that during annealing $BaCl_2$ crystals have been formed because the annealed samples no longer exhibit the crystallization peak associated with the formation of $BaCl_2$ crystals.

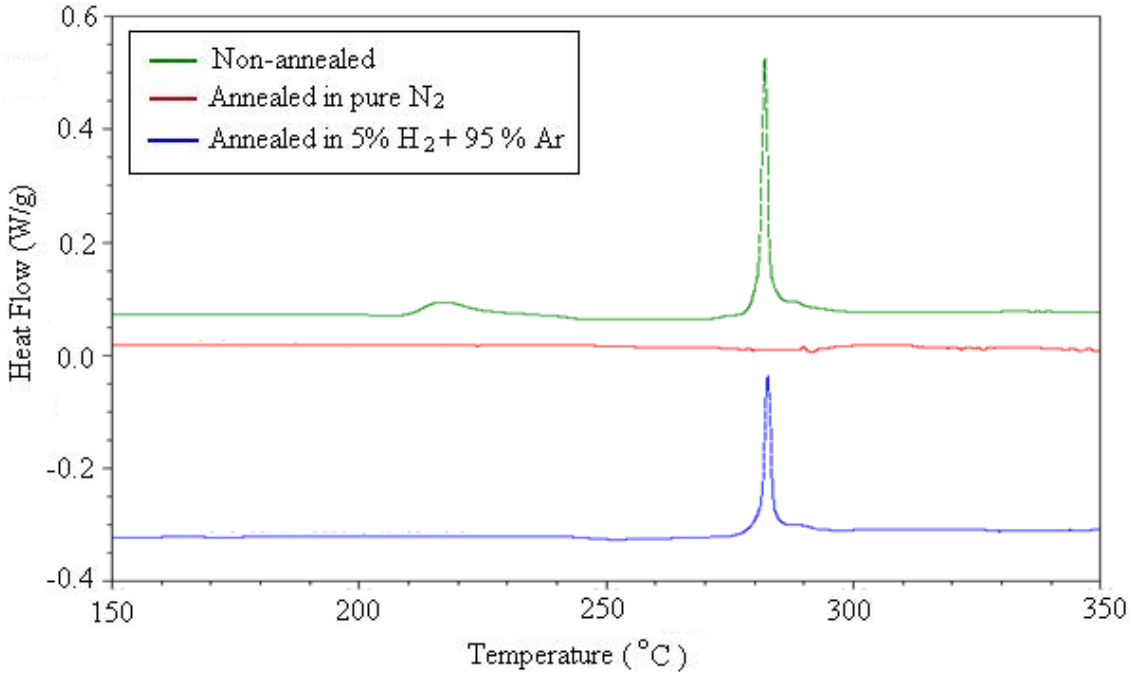

Figure 4.18. DSC of non annealed and annealed Sm^{3+} doped FCZ glass samples with 13% relative Cl-content at 250 ^{o}C for 30 mins.

4.2.2.3. Influence of annealing parameters on nanocrystals

The annealing temperature and time are important parameters in controlling the formation and growth of nanocrystals. Figure 4.19 shows a DSC thermogram of a non-annealed 1% Sm doped FCZ glass sample versus that of an annealed (at 270 °C for 30 minutes in a 5% H_2, 95% Ar gas mixture) 1% Sm-doped FCZ glass sample.

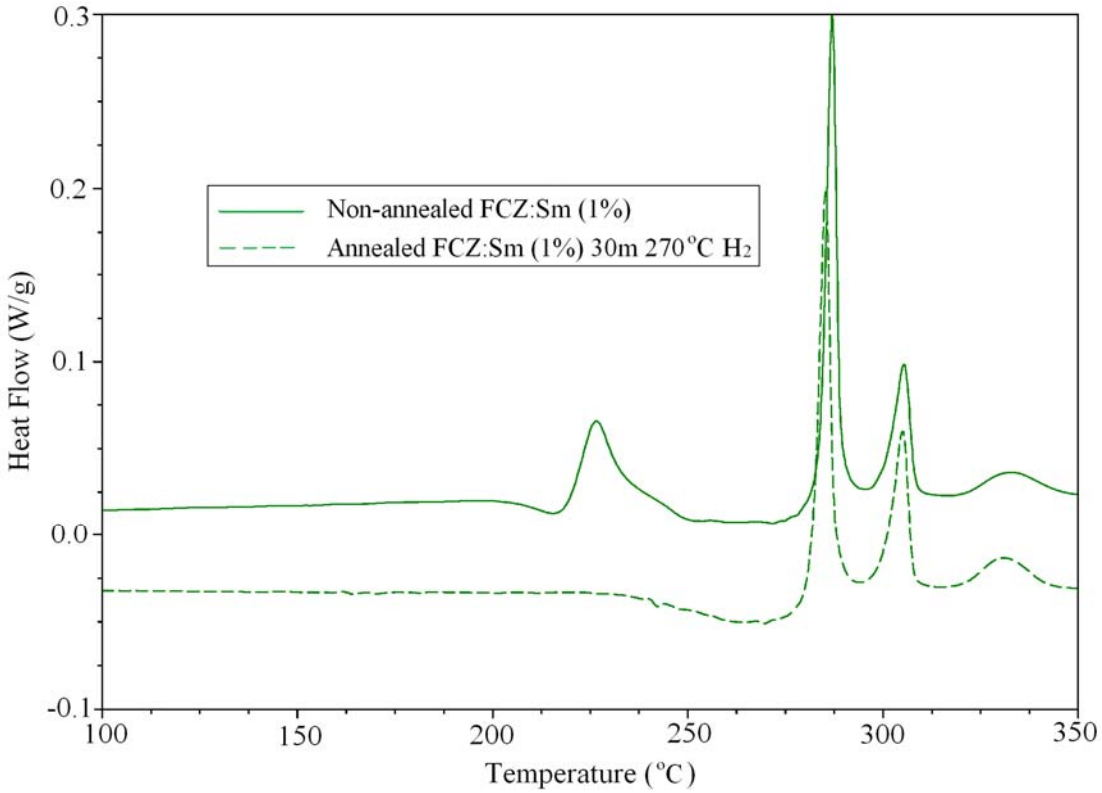

Figure 4.19. DSC heat flow vs. temperature curves of non-annealed and annealed FCZ : Sm (1%) glass samples to form a transparent nanocrystalline Sm-doped FCZ glass-ceramic material.

The first scan (for non-annealed 1% Sm doped FCZ glass sample) has an exothermic crystallization peak roughly at 225 °C. The exothermic peaks at about 280 °C correspond to the crystallization of the glass host. Annealing at high temperatures can easily lead to the crystallization of the whole glass. For example, samples annealed at temperatures higher than 275 ^{o}C for 30 minutes are opaque (white) polycrystalline materials while samples annealed at 250 ^{o}C or below 275 ^{o}C are transparent and similar to the non-annealed glasses. The annealing in this temperature interval (250 ^{o}C - 275 ^{o}C) allows the Cl-rich phase to crystallize and form luminescence active nanocrystals in the glass matrix. It is important to maintain the material transparency for practical

applications, which means that annealing temperatures and times must be chosen carefully. The chosen temperatures are above the lowest crystallization ($BaCl_2$) peak and sufficiently below the main crystallization peak of the FCZ glass material.

5. CONCLUSIONS AND RECOMMANDATIONS

5.1. Conclusions

Thermal and optical properties of rare earth doped and undoped FCZ glasses with different amounts of relative halogen (Cl) concentration, expressed as [Cl] / [Cl+F] have been investigated and compared with carrying out infrared spectroscopy, photoluminescence, X-ray luminescence, heat treatment and annealing experiments, conventional differential calorimetry (DSC), modulated differential calorimetry (MDSC) methods.

5.1.1. Thermal properties

In DSC and MDSC methods, thermal stability of both the rare earth doped and undoped FCZ glass samples were investigated.

1. It is found that, depending on the relative Cl-content, both the glass samples can have a two-phase structure.
2. The observation of two possible glass transition temperatures by modulated temperature differential scanning calorimetry (MDSC) indicates the presence of two phases in the glasses contain higher R_{Cl} content.

3. It is observed that the changes in T_gs and C_ps are not related with the amounts of rare earth doping but depend on different amounts of relative chlorine content and arising from the chloride salts of Eu and Sm ions.
4. The heat capacity values are evaluated at two different fixed temperatures. Heat capacity values increase with increasing relative halogen content in both Sm^{3+} and Eu^{2+} doped FCZ glass samples.

Kissinger plots for both doped and undoped FCZ glass samples shows that doping leads to a slight increase in the activation energy. It can be said that the doped FCZ glass sample having higher activation energy is thermally more stable than the undoped FCZ glass sample. However, the difference in the actication energies is small.

5.1.2. Optical properties

In the optical properties of the rare-earth doped FCZ glasses were examined by measuring their transmission spectra. It is found that FCZ glass samples can be a possible hosts for doping with rare earth elements

1. Doped and annealed FCZ glass samples exhibit better transparency, absorb less and are thermally more stable.

2. The x-ray luminescence and photluminescence spectra from Sm-Doped FCZ glasses represented the luminescence spectra of Sm^{3+} ions. In both cases the luminescence spectra were the same though the two processes involve different excitation processes.

3. The integrated PL intensity increased linearly with the Sm-concentration whereas the integrated x-ray luminescence intensity exhibited sublinear dependence. The

difference is likely to be due to the different mechanisms involved in the exciation of the Sm^{3+}-ions.

4. Good correlation between X-ray luminescence intensity and the changes in the structure, monitored through the heat capacity, is observed. The correlation is not unexpected if the excitation of the x-ray luminescence involves the bulk glass.

5. It is observed that the relative halogen content [Cl/(Cl+F) %] not only affects thermal properties as observed in DSC and MDSC results on FCZ glass samples but also affects their X-ray luminescence and photoluminescence properties.

5.1.3. The importance of annealing

The importance of establishing appropriate annealing conditions (temperature, time and ambient atmosphere) has been examined. It is observed that:

1. The annealing process significantly increases the magnitude of the X-ray luminescence and photoluminescence signals compared to the one observed in the corresponding unprocessed or non annealed glass sample.

2. Annealing in the presence of hydrogen has a strong effect on X-ray luminescence properties of FCZ glass sample materials. It is observed that by annealing FCZ doped samples for 30 minutes at 250 ^{o}C in reducing atmosphere (a mixture of 5 % H_2 + 95 % Ar) gives a higher X-ray luminescence signal than those samples annealed under an inert atmosphere (N_2).

3. It is also noticed that the samples annealed in the presence of hydrogen tend to remain transparent while the samples annealed in nitrogen under the same conditions lose their transparency and appear white.

5.2. Recommendations

1. Preparation conditions and glass matrix should be optimized to get a better performance.
2. Annealing conditions should be optimized in order to get the desired nanocrystals in the glass matrix.
3. Concentrations of Eu^{2+} and Sm^{3+} dopants should be optimized to obtain more efficient scintillators.
4. Annealing in the presence of hydrogen improves the x-ray luminescence signal and practically eliminates the storage properties of the material (phosphor effect) which can be considered as a technological advantage.

REFERENCES

[1] D. Tucker and J. M. Horace, "Effects of gravity on processing heavy metal fluoride fibers," *Journal of Materials Research*, vol. 12, no. 9, pp. 2223-2225, 1997.

[2] M. Poulain, M. Poulain, and J. Lucas, "Verres fluores au tetrafluorure de zirconium propretés optiques d'un verre dope au Nd^{3+}," *Materials Research Bulletin*, vol. 10, no. 4, pp. 243-246, 1975.

[3] D. Tonchev and S.O. Kasap, "Thermal characterization of glasses and polymers by temperature modulated differential scanning calorimetry: glass transition temperature," in *High Performance Structures and Materials II*, C.A. Brebbia and W.P. De Wilde, Eds. WIT Press, UK, pp. 223-231, 2005.

[4] M.G. Drexhage, C.T. Moynihan, B. Bendow, E. Gboji, K.H. Chung and M. Boulos, "Influence of processing conditions on IR edge absorption in fluorohafnate and fluorozirconate glasses," *Materials Research Bulletin*, vol.16, no. 8, 933-941, 1981.

[5] B. Bendow, R. N. Brown, M. G. Drexhage, T. J. Loretz, and R. L. Kirk, "Material dispersion of fluorozirconate-type glasses," *Applied Optics,* vol. 20, no. 21, pp. 3688-3690, 1981.

[6] D. Tonchev, G. Belev, C. Koughia, S. Panigrahi, C. Varoy, A. Edgar and S.O.Kasap, "Thermally Induced Nanostructures in Samarium-Doped Glass Ceramics for X-Ray Sensor Applications," in *Nanotechnological Basis for Advanced Sensors,* J.P. Reithmaier, P. Petkov, W. Kulich and C. Popov, Eds., pp. 241-248, 2011.

[7] C. J. Simmons, H. Sutter, J. H. Simmons, and D. C. Tran, "Aqueous corrosion studies of a fluorozirconate glass," *Materials Research Bulletin*, vol. 17, no.9, pp. 1203-1210, 1982.

[8] L. Wetenkamp, G.F West and H. Többen, "Optical properties of rare earth-doped ZBLAN glasses" *Journal of Non-Crystalline Solids*, vol. 140, pp. 35-40, 1992.

[9] Y. Huang, C. Jiang, K. Jang, H.S. Lee, E. Cho, M. Yayasimhardi, and S.S. Yi, "Luminescence and microstructure of Sm^{2+} ions reduced by x-ray irradiation in$Li_2O–SrO–B_2O_3$ glass," *Journal of Applied Physics*, vol.103, no. 11, pp. 113519.1-7, 2008.

[10] J.C. Duan, W.F. Li, X.Y Wu, H.H. Chen, X.X Yang and J.T. Zhao, "Syntheses and X-ray excited luminescence properties of $Ba_3BP_3O_{12}$, $BaBPO_5$ and Ba_3BPO_7," *Journal of Luminescence*, vol.117, no.1, pp. 83-89, 2006.

[11] A. Edgar, G.V.M. Williams, P.K.D. Sagar, M. Secu, S. Schweizer, J.M. Spaeth, X. Hu, P.J. Newman and D.R. MacFarlane, "A new fluorozirconate glass-ceramic X-ray storage phosphor," *Journal of Non-Crystalline Solids*, vol. 326-327, pp. 489-493, 2003.

[12] M. Thoms and H. Von Seggern, "Method for the determination of photostimulable defect and effective formation energies," *Journal of Applied Physics*, vol. 75, no. 9, pp. 4658-4661, 1994.

[13] S. Schweizer, L. W. Hobbs, M. Secu, J.-M. Spaeth, A. Edgar, and G. V. A. Williams, "Photostimulated luminescence in Eu-doped fluorochlorozirconate glass ceramics," *Applied Physics Letters*, vol. 83, no. 3, pp. 449-451, 2003.

[14] A. Edgar, S. Schweizer, S. Assmann, J. M. Spaeth, P. J. Newman, and D. R. MacFarlane, "Photoluminescence and crystallization in europium-doped fluorobromozirconate glass-ceramics," *Journal of Non-Crystalline Solids*, vol. 284, no. 1-3, pp. 237-242, 2001.

[15] D. C. Tran, C. F. Fisher and G. H. Sigel, "Fluoride glass preforms prepared by a rotational casting process," *Electronics Letters,* vol. 7, no. 15, pp. 657-658, 1992.

[16] H. Malik and K. Maqsood, "Effect of distilled water on the optical properties and surface degradation of Zr-Ba based glass." *Journal of Materials Science*, vol. 37, no. 24, pp. 5367-5369, 2002.

[17] D. C. Tran, K. H. Levin, C. F. Fisher, M. J. Burk, and G. H. Sigel, "Rayleigh scattering in fluoride glass optical fibres, "*Electronics Letters,* vol. 19, no. 55, pp. 165-166, 1983.

[18] C. J. Simmons and J. H. Simmons, "Chemical Durability of Fluoride Glasses: I, Reaction of Fluorozirconate Glasses with Water," *Journal of the American Ceramic Society,* vol. 69, no. 9, pp. 661-669, 1986.

[19] C. Jijian, Z. Rong and E. G. Rakov, Water resistance of cadmium-containing fluorozirconate glasses," *Journal of Non-Crystalline Solids,* vol. 112, no. 1-3, pp. 392-398, 1989.

[20] Dennis S. Tucker, Gary L. Workman, and Guy A. Smith, "Effects of gravity on processing heavy metal fluoride fibers," *Journal of Materials Research*, vol.12, no.9, pp. 2223-2225, 1997.

[21] K. Kincade, "Optoelectronics Application: Biophotonics," *Fiber lasers find opportunities in medical applications*, vol. 41, pp.9, 2005.

[22] D. Dooling, "ZBLAN has great commercial potential" http://science.nasa.gov/search/?q=ZBLAN, and date access May 23, 2011.

[23] M. J. Dejneka, "Transparent oxyfluoride glass ceramics," *Materials Research Society Bulletin*, vol. 23, no. 11, pp. 57, 1998.

[24] A. Edgar, G. V. M. Williams, S. Schweizer, and J. M. Spaeth, "Spatial resolution of a glass-ceramic x-ray storage phosphor," *Current applied physics*, vol. 6, no. 3, pp. 399-402, 2006.

[25] G. Hohne, W. Hemminger and H. J. Flammersheim, "Differential Scanning Calorimetry," Springer-Verlag, Germany, pp. 9-241, 1996.

[26] M. Takahashi, R. Yamamoto, R. Kanno, and Y. Kawamoto, "Molecular dynamics simulation of Eu^{3+}-doped chlorofluorozirconate glasses," *Journal of Physics: Condensed Matter* , vol.7, no. 24, pp. 4583-4592, 1995.

[27] A. Edgar, G.V.M. Williams, P.K.D. Sagar, M. Secu, S. Schweizer, J.M. Spaeth, X. Hu, P.J. Newman and D.R. MacFarlane, "A new fluorozirconate glass-ceramic X-ray storage phosphor," *Journal of Non-Crystalline Solids,*, vol. 326-327, pp. 489-493, 2003.

[28] H. Inoue, K. Soga, A. Makashima, and I. Yasui, "Structure of 50Na20.xA1203.(50-x)P205 and (50-x/2)Na20.xA1z03 (50-x/2)P20S glasses," *Physics and Chemistry of Glasses,* vol. 36, pp. 1-5, 1995.

[29] K. Soga, H. Inoue, and A. Makashima, "Calculation and simulation of spectroscopic properties for rare earth ions in chloro-fluorozirconate glasses," *Journal of Non-Crystalline Solids,* vol. 274, pp. 69-74, 2000.

[30] S.C. Hendy and A. Edgar, "Structure of fluorochlorozirconate glasses using molecular dynamics," *Journal of Non-Crystalline Solids*, vol. 352, pp. 415-422, 2006.

[31] DSC 2910 Differential Scanning Calorimetry, *TA Instruments Manual,* 1994.

[32] S. O Kasap and D. Tonchev, "Glass transformation in vitreous As2Se3 studied by conventional and temperature-modulated differential scanning calorimetry", *Journal of Materials Research*, vol. 16, no. 8, pp. 2399-2407, 2001.

[33] D. Tonchev, S. Panigrahi, G. Belev, C. Koughia, C. Varoy, A. Edgar, and S.O. Kasap, "Glass Transition and Crystallization Properties of Eu- and Sm-doped fluorochlorozirconate glasses studied by DSC and TMDSC," 16th International Symposium on Non oxide and New Optical Glasses (ISNOG16), Montpellier, France. 2008.

[34] A. Boiler, Y Jin and B. Wunderlich, "Heat capacity measurement by modulated DSC at constant temperature," *Journal of Thermal Analysis and Calorimetry*, vol.42, no. 2-3, pp. 307-330, 1994.

[35] Modulated DSC^{TM} Compendium, *TA Instruments Manual*, 1994.

[36] L. Hwa and C. Shu, "The structural Investigation of a ZBLAN Glass by Vibrational Spectroscopy," *Chinese Journal of Physics*, vol. 34, pp.1270-1275, 1996.

[37] J. D. Yang and L. G. Hwa, "Raman Scattering in Multicomponent halide Glasses", Chinese J. Materials Science, Vol 26, no. 4, 319-322, 1994.

[38] G. Soundararajan, "Optical characterization of rare earth doped glasses," Master's thesis, University of Saskatchewan, 2009.

[39] Go Okada, "Optical Properties of Rare-Earth doped Fluorozirconate Glass-Ceramics for X-Ray Detector Applications", Master's thesis, University of Saskatchewan, 2010.

[40] Allen, D., Cooksey, C., & Tsai, B., "Spectrophotometry," Retrieved from http://www.nist.gov/pml/div685/grp03/spectrophotometry.cfm 05-October, 2010.

[41] G. Schwedt, "The Essential Guide to Analytical Chemistry,"NY: Wiley, pp.16-17, 1997.

[42] D. Tonchev, G. Belev, S. Panigrahi, C. Varoy, A. Edgar, H. Von Seggern, S.O. Kasap, "Rare-Earth Doped Fluorochlorozirconate (FCZ) Glasses and Glass-Ceramics: Selected Thermal Properties and X-Ray Luminescence in Samarium Doped FCZ," in *Nanostructured Materials for Advanced Technological Applications,* NATO Science for Peace and Security Series – B: Physics and Biophysics, J.P. Reithmaier, P. Petkov, W. Kulich and C. Popov, Eds., Springer, Netherlands, pp. 377-391, 2009.

[43] B. Henke, B. Ahrens, P. T. Miclea, C. Eisenschmidt, J. A. Johnson, and S. Schweizer, "Erbium- and chlorine-doped fluorozirconate-based glasses for upconverted fluorescence," *Journal of Non-Crystalline Solids*, vol. 355, pp.1916-1918, 2009.

[44] Edgar, A., Williams, G.V.M., Secu, M., Schweizer, S., and Spaeth, J.-M., "Optical properties of a high-efficiency glass ceramic X-ray storage phosphor," *Radiation Measurements*, vol.38 no. 4-6, pp. 413-416, 2004.

[45] S. Schweizer and J. A. Johnson, "Fluorozirconate-based glass ceramics x-ray detectors for digital radiography," *Radiation Measurements,* vol. 42, pp. 632-637, 2006.

[46] T. Wagner and S. O. Kasap, "Glass transformation, heat capacity and structure of AS_xSe_{1-x} glasses studied by modulated temperature differential scanning calorimetry experiments," *Philosophical Magazine B*, vol. 74, no. 6, pp. 667-680, 1996.

[47] M. Overdick, "Detectors for x-ray imaging and computed tomography," in *Advance in Healthcare Technology – Shaping the*

Future of Medical Care, G. Spekowius and T. Wendler, Eds. The Netherlands: Springer, pp. 49-64, 2006.

[48] S.O. Kasap and C. Juhasz, "Theory of thermal analysis of non-isothermal crystallization kinetics of amorphous solids," *Journal of the Chemical Society, Faraday Transactions 2: Molecular and Chemical Physics,* vol. 81, pp. 811-831, 1985.

[49] M. Munzar, C. Koughia, D. Tonchev, K. Maeda, T. Ikari, C. Haugen, R. Decorby, J.N. McMullin, S.O. Kasap, "Optical properties of Er-doped Gax (Ge0.3Se0.7) 100-x glasses," *Optical Materials*, vol.28, no. 3, pp. 225-230, 2006.

[50] S. Panigrahi, D. Tonchev, S.O. Kasap, C. Varoy and A. Edgar, "Properties of Flurochlorozirconate Glasses (FCZ) with varying Cl/F fractions," *14 ISCMP*, Varna, Bulgaria, September 17-22, 2006.

[51] A. Edgar, G. Williams, and J. Hamlin, "Photostimulated luminescence from fluorochlorozirconate glass ceramics and the effect of crystallite size," *Journal of Applied Physics,* vol. 97, pp.93522, 2005.

[52] S. Schweizer, S. Hobbs, L. Secu, M. Spaeth, J-M. Edgar, A. and G.V.M. Williams, "Photostimulated luminescence in Eu-doped fluorochlorozirconate glass ceramics", *Applied Physics Letters*, vol. 83, pp. 449-451, 2003.

[53] J. A. Johnson, D. Holland, J. Urquidi, I. A. Gee, C. J. Benmore and C. E. Johnson, "Structure of oxychloride glasses by neutron and x-ray difference and XPS," *Journal of Physics: Condensed Matter*, vol.15 no. 27, pp. 4679-4693, 2003.

[54] http://en.wikipedia.org/wiki/Transparency_and_translucency, and date of access: May 23, 2011.

[55] G. Chen, J. Johnson, R. Weber, R. Nishikawa, S. Schweizer, P. Newman, and D. MacFarlane, "Fluorozirconate-based nanophase glass ceramics for high resolution medical x-ray imaging," *Journal of Non-Crystalline Solids*, vol. 352, no. 6-7, pp. 610-614, 2006.

[56] M. Takahashi, R. Kanno, Y. Kawamoto, and K. Kadono, "Local structure around Zr^{4+} in ZrF_4-BaF_2-$BaCl_2$-EuF_3 glasses", *Journal of Physics: Condensed Matter*, vol. 7, no. 40, pp. 7797-7804, 1995.

[57] H. Huang, C. Jiang, K. Jang, H.S. Lee, E. Cho, M. Yayasimhardi, and S.S. Yi, "Luminescence and microstructure of Sm^{2+} ions reduced by x-ray irradiation in $Li_2O–SrO–B_2O_3$ glass," *Journal of Applied Physics,* vol.103, pp. 113519, 2008.

[58] J.C. Duan, W.F. Li, X.Y Wu, H.H. Chen, X.X Yang, J.T. Zhao, "Syntheses and X-ray excited luminescence properties of $Ba_3BP_3O_{12}$, $BaBPO_5$ and Ba_3BPO_7," *Journal of Luminescence,* vol. 117, no.1 pp. 83, 2006.

[59] Spectrophotometer, http://en.wikipedia.org/wiki/Spectroscopy, and date access October 25 2009.

[60] Wee Chong Tan, "Optical Properties of Amorphous Selenium Films," Master's thesis, University of Saskatchewan, 2006.